Dynamic simulation, optimisation AND ECONOMIC ANALYSIS of FED-BATCH vs. perfusion bioreactors for advanced mAb manufacturing

DYNAMIC SIMULATION, OPTIMISATION AND ECONOMIC ANALYSIS OF FED-BATCH vs. PERFUSION BIOREACTORS FOR ADVANCED mAb MANUFACTURING

Wil Jones, Dimitrios I. Gerogiorgis[a*]

Institute for Materials and Processes (IMP), School of Engineering, University of Edinburgh, The Kings Buildings, Edinburgh, EH9 3FB, Scotland, U.K.

[*]*Corresponding Author*: D.Gerogiorgis@ed.ac.uk (*+44 131 6517072*)

Keywords: Dynamic Simulation; Dynamic Optimisation; Biopharmaceutical manufacturing

ABSTRACT

The variation of antigen binding sites on monoclonal antibodies (mAbs) enables manufacturing of the latter for targeted treatment of a variety of ailments, including cancer types and autoimmune diseases. Fed-batch operation of biochemical reactors used to manufacture mAbs grants the ability to manipulate cell dynamics via intermittent feeding of nutrients/substrates. Regulatory authority agendas (e.g. the U.S. Food & Drug Administration) consider the development of continuous technologies (e.g. perfusion reactors) as essential towards improved economic potential and biopharmaceuticals quality control.

This paper presents dynamic simulations for a fed-batch and a perfusion reactor, in which a hybridoma cell culture is used to secrete mAb glycoforms. A novel dynamic optimisation of the fed-batch and perfusion reactors is conducted towards maximising the total mAb mass produced. Nonlinear Programming (NLP) formulations with the use of APOPT and IPOPT solvers provide the manipulation, state and controlled variable trajectories, to achieve this objective. The technoeconomic analysis clearly highlights strong benefits for the fed-batch bioreactor (especially over a plant-life time horizon), but also showcases a cost-related promise of perfusion bioreactor technologies, given the higher mAb yield.

1. Introduction

1.1 Monoclonal antibodies

Monoclonal antibodies (mAbs) are protein molecules which are engineered within laboratories to serve as substitutes for antibodies produced by human plasma cells (Goding, 1996; Bayer, 2019). The structure of mAbs (Fig. 1) consists of four polypeptide chains; two identical heavy chains and two identical light chains which are linked up together with disulphide bonds (Spearman et al., 2011). The constant "Fc" region consists of the two heavy chains and is responsible for linking the antibody with immune response cells. The two heavy chains and two light chains make up the variable "Fab" region responsible for targeting and binding to antigens (Ahangarzadeh et al., 2020). The mechanism which the antibody uses attach to antigens is specific to the binding region (Chames et al., 2009). Examples of different binding mechanisms include (amongst others) TNF alpha antagonist for Infliximab, CD20 for Rituximab and HER2 for Trastuzumab (Scott et al., 2012; Kantardjieff et al., 2013).

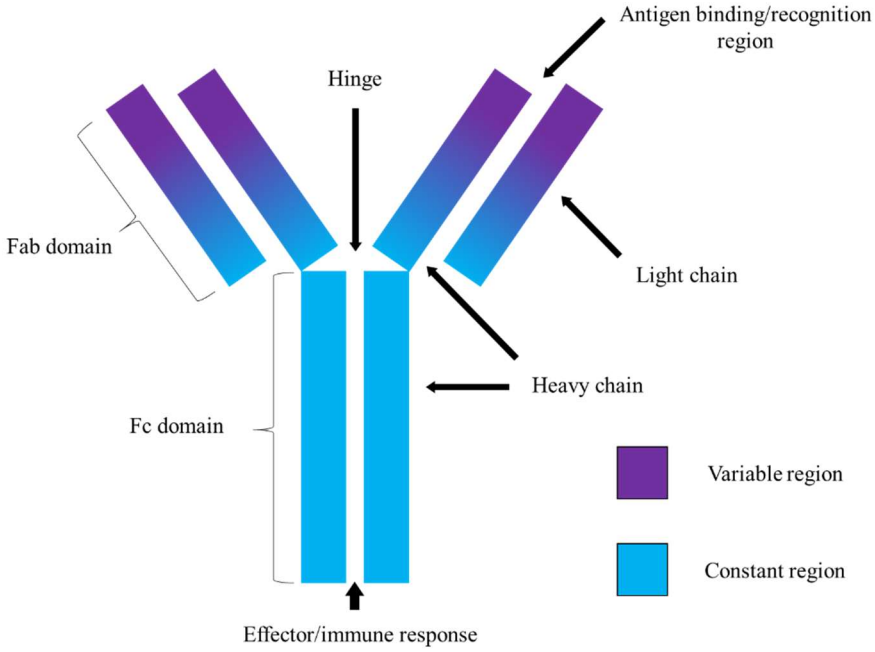

Figure 1. Monoclonal antibody structure (Saeed et al., 2016).

The presence of the variable region allows for numerous antigens to be targeted and neutralised if these mAb molecules are formulated effectively (Mahmuda et al., 2017). Commercially available mAbs already exist to allow for patient treatment of ailments such as chronic lymphocytic leukemia with Rituximab (Furman et al., 2014), diabetic macular edema with Ranibizumab (Wells et al., 2015) and crohn's disease with Adalimumab (Colombel, et al. 2007).

1.2 Market insights of mAbs

The United States Food and Drug Administration (FDA) approved *muromonab-CD3* in 1986, thus making it the first therapeutic mAb to ever receive approval for commercial use (Kesik-Brodacka, 2018). Following this historic milestone there have been many (78) more mAbs approved for patient usage (Lu et al., 2020) and the mAb product type now contributes approximately 21 % of total approved biologics (Kantardjieff et al., 2013). Currently, mAbs are the fastest growing biopharmaceutical product type; they represented 27 % of total biopharmaceutical approvals from 2010 to 2014 and 57 % of total biopharmaceutical approvals between 2015 and 2018 (Ecker et al., 2015; Walsh, 2018). Despite there being a relative stagnation in mAb approval of only 16 mAbs between 2002 and 2012, the period between 2012 and 2017 led to 35 novel mAbs being given market approval by the FDA and European Medicines Agency (EMA) (Nelson et al., 2010; Grilo et al., 2019), (Fig. 2).

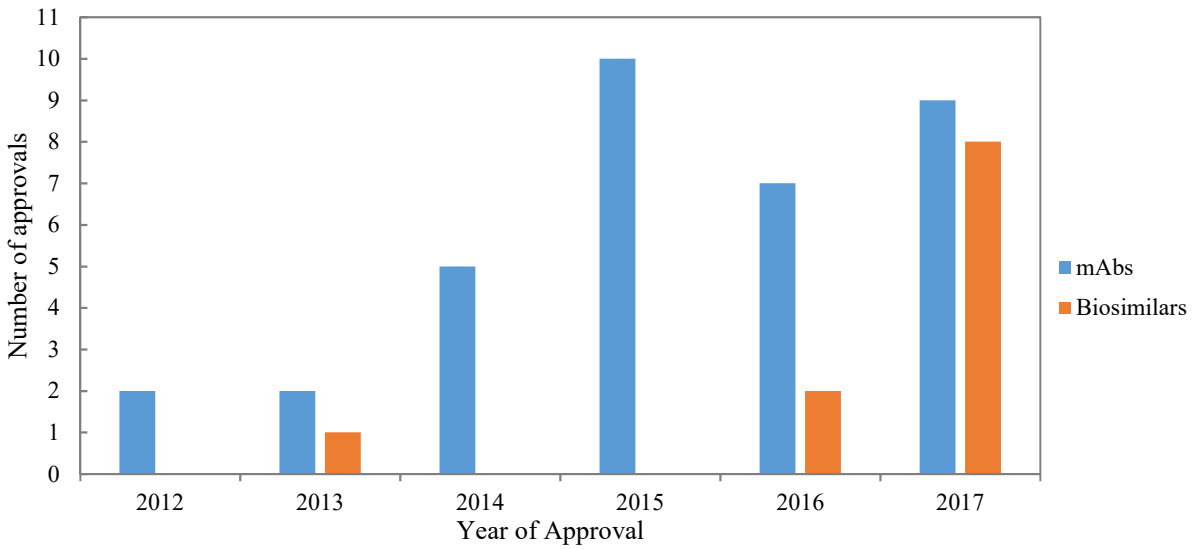

Figure 2: Recent approvals by the FDA and EMA (Grilo et al., 2019).

1.3 This work

The commercial viability of mAbs which are in early development stages is highly dependent on the technoeconomic performance of the industrial scale manufacturing process (Badr and Sugiyama, 2020). The incentive to improve patient wide access to these biotherapeutics drives the need for accurate *in silico* techniques to dynamically simulate reactions to understand metabolic networks (Morchain and Fonade, 2009; Lira-Parada et al., 2021; Mannina et al., 2021). These keen pursuits motivate the need for dynamic optimisation to be applied to upstream processes, so as to provide control strategies for improved culture productivity (Bibila and Robinson, 1995). Dynamic simulation, optimisation and technoeconomic analyses attest to the ever-increasing importance of PSE tools for biopharmaceutical manufacturing (Shirahata et al., 2019; Diab et al., 2020; Badr and Sugiyama, 2020), especially for equipment selection (Zürcher et al., 2020) and LCA (Amasawa et al., 2021). Continuous methods are of particular interest (Gerogiorgis and Barton, 2009; Gerogiorgis and Jolliffe, 2015; Diab et al., 2019).

A published process model (De Tremblay, et al. 1992) is employed here for dynamic simulation of two bioreactors, one operating in fed-batch mode and one operating in continuous steady state mode in order to analyse metabolic interactions. Dynamic optimisation is then performed to elucidate optimal feeding, bleeding and harvest strategies to enhance mAb production in the fed-batch and continuous steady state bioreactors. An economic analysis for the implementation and operation of these two bioreactors is then presented, to visualise their viability for rapid scale up. Finally, a discussion summarises our findings from simulation and optimisation study, and details conclusions from technoeconomic comparisons.

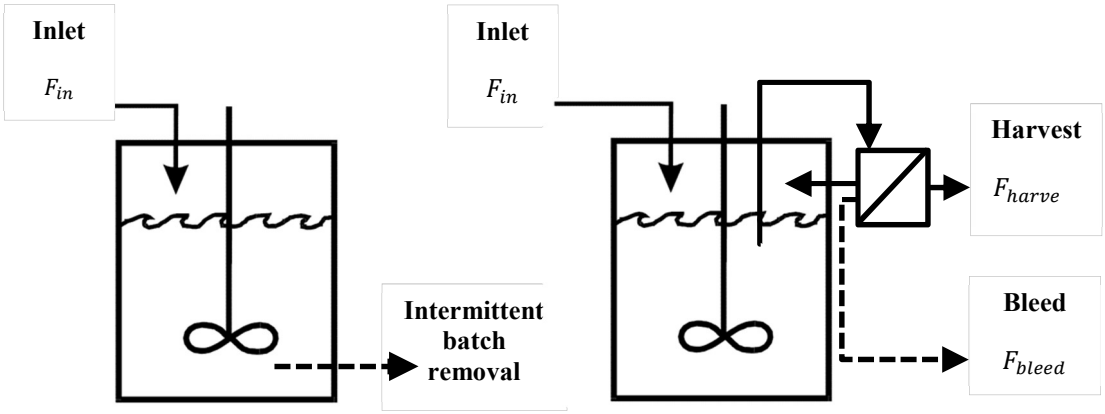

Figure 3: A diagram sketch of the fed-batch reactor (left) and the perfusion reactor (right).

2. Methodology

2.1 Dynamic process modelling

The process model considered is published by De Tremblay et al. (1992) and has been employed in many recent studies (Nguang et al., 2001; Chen and Wang, 2004; Franco-Lara and Weuster-Botz, 2005; Sbarciog et al., 2014; Saraiva et al., 2015; Mutturi, 2018). The present paper considers how a hybridoma cell line can be applied in fed-batch and perfusion bioreactors for mAb manufacturing, and how inlet flows can be manipulated to optimise bioreactor performance. The model reaction kinetics consider 7 state variables, 2 control variables, 8 algebraic equations and 16 parameters. The mass balances formed in the process model assume perfect mixing of a STR and negligible lag phase of growth. Perfect mixing allowed temperature, pH and dissolved oxygen to all be controlled, these factors are thus not considered in the model (Newell et al., 1998; Woodside et al., 1998). Lastly, an assumption that the concentration of reactor contents was homogenised and uniform throughout was made due to the small volume and agitated nature of the vessels (Okkels et al., 2011). The inlet to the reactor contained glucose and glutamine, both of which have been shown to benefit the specific growth rates of hybridoma cell lines (De Tremblay, et al. 1992). It is important to note that no active cells were fed to the reactors via the inlet flow. Schematic diagrams for fed-batch and perfusion modes of operation can be seen in Figure 3 (Woodside et al., 1998). The simulation here considers the fed-batch operation with one inlet feed and without outlet flow (the intermittent batch removal takes place outside the considered time domain).

Table 1: A summary of the system of equations used to formulate the fed-batch reactor simulation.

Volume	$\frac{dV}{dt} = F_{in}$	(1)
Viable cell density	$\frac{d[X_V]}{dt} = (\mu - k_d)X_V - \frac{(F_{in})}{V}X_V$	(2)
Glucose concentration	$\frac{d[GLC]}{dt} = (GLC_{in} - GLC)\frac{F_{in}}{V} - q_{GLC}X_V$	(3)
Glutamine concentration	$\frac{d[GLN]}{dt} = (GLN_{in} - GLN)\frac{F_{in}}{V} - q_{GLN}X_V$	(4)
Lactate concentration	$\frac{d[LAC]}{dt} = q_{LAC}X_V - \frac{F_{in}}{V}LAC$	(5)
Ammonia concentration	$\frac{d[AMM]}{dt} = q_{AMM}X_V - \frac{F_{in}}{V}AMM$	(6)
mAb concentration	$\frac{d[mAb]}{dt} = q_{mAb}X_V - \frac{F_{in}}{V}mAb$	(7)

Table 2: Summary of the model parameters (De Tremblay, et al. 1992).

Definition	Symbol	Value	Unit
Maximum specific growth rate	μ_{max}	1.09	day^{-1}
Yield of viable cells from glucose	$Y_{Xv,GLC}$	$1.09 \cdot 10^{8}$	$(10^6$ cell) $mmol^{-1}$
Glucose cell maintenance term	m_{GLC}	$0.17 \cdot 10^{-2}$	mmol $(10^6$ cell$)^{-1}$ day^{-1}
Monod constant for glucose based cell growth	K_{GLC}	1.0	mmol L^{-1}
Luedeking-Piret alpha constant	α_0	$2.57 \cdot 10^{-2}$	mg $(10^6$ cell$)^{-1}$ day^{-1}
Luedeking-Piret beta constant	β	$0.35 \cdot 10^{-2}$	mg $(10^6$ cell$)^{-1}$ day^{-1}
Ammonia growth inhibition constant	$k_{d,AMM}$	0.06	day^{-1} $mmol^{-1}$ L
Yield of lactate from glucose metabolism	$Y_{LAC/GLC}$	1.8	mmol $mmol^{-1}$
Maximum specific death rate	$k_{d,max}$	0.69	day^{-1}
Yield of viable cells from glutamine	$Y_{Xv/GLN}$	$3.8 \cdot 10^{2}$	$(10^6$ cell) $mmol^{-1}$
Monod constant for glucose cell maintenance	$k_{m,GLC}$	19.0	mmol L^{-1}
Monod constant for glutamine cell growth	K_{GLN}	0.3	mmol L^{-1}
Luedeking-Piret growth constant	k_μ	0.02	day^{-1}
Lactate growth inhibition constant	$k_{d,LAC}$	0.01	day^{-1} $mmol^{-1}$ L
Glutamine growth inhibition constant	$k_{d,GLN}$	0.02	mmol L^{-1}
Yield of ammonia from glutamine metabolism	$Y_{AMM/GLN}$	0.85	mmol $mmol^{-1}$

The perfusion simulation was computed to have one inlet flow and one outlet flow. This outlet flow is split into harvest flow (a flow containing no cells, just an effluent mixture) and bleed flow (containing both cells and reactor effluent). Woodside et al. (1998) provides a comprehensive overview of perfusion technologies, which was used as a basis in this study.

2.2 Fed-batch reactor modelling

A complete overview of the system of equations describing the fed-batch reactor can be seen in Table 1. The inlet flow consisted of glucose and glutamine substrates, these were assumed to have equal contribution to cellular growth and were modelled to be multiplicative to specific growth rate. Consumption of both substrates was assumed to be a function of cellular yield, however glucose was also considered to be used in culture maintenance whilst glutamine was not. Lactate and ammonia productivity rates were taken as proportional to the productivities of glucose and glutamine respectively. Lastly, mAb production was assumed to take the form of a Luedeking-Piret model, a classic framework for antibody production (Luedeking and Piret, 2000). A summary of the intermediate equations and the model parameters values can be seen in Table 2 and 3 respectively.

Table 3: Intermediate expressions for the system of equations (De Tremblay, et al. 1992).

$$\boldsymbol{\mu = \mu_{max}\left(\frac{GLC}{GLC + K_{GLC}}\right)\left(\frac{GLN}{GLN + K_{GLN}}\right)} \quad (8)$$

$$\boldsymbol{k_d = k_{d,max}\left(\mu_{max} - k_{d,LAC}\cdot [LAC]\right)^{-1}\left(\mu_{max} - k_{d,AMM}\cdot [AMM]\right)^{-1}\frac{k_{d,GLN}}{k_{d,GLN} + [GLN]}} \quad (9)$$

$$\boldsymbol{q_{GLN} = \frac{\mu}{Y_{Xv/GLN}}} \quad (10)$$

$$\boldsymbol{q_{GLC} = \frac{\mu}{Y_{Xv/GLC}} + m_{GLC}\left(\frac{GLC}{GLC + k_{m,GLC}}\right)} \quad (11)$$

$$\boldsymbol{q_{LAC} = Y_{LAC/GLC}\cdot q_{GLC}} \quad (12)$$

$$\boldsymbol{q_{AMM} = Y_{AMM/GLN}\cdot q_{GLN}} \quad (13)$$

$$\boldsymbol{q_{mAb} = \left(\frac{\alpha_o}{k_\mu + \mu}\right)\cdot \mu + \beta} \quad (14)$$

2.3 Perfusion reactor modelling

A full equation list for the perfusion reactor system can be seen below in Table 4. A key difference between the fed-batch system and this system is there is an outlet flowrate, consisting of a bleed flow and a harvest flow. As stated in subsection 2.2, the intermediate equations and model parameters values have been summarised in Table 2 and 3 respectively. In practice the bleed rate is used to maintain the cell viability within the reactor at a desired set point value. Consequently, the bleed rate from the reactor was set as a function of cellular growth and medium volume in order to keep the cellular concentration at an adequate level for sizeable product yield.

Table 4: A summary of the system of equations used to formulate the perfusion reactor simulation.

Volume	$\frac{dV}{dt} = F_{in} - F_{out}$	(15)
Outlet flowrate	$F_{out} = F_{bleed} + F_{harvest}$	(16)
Viable cell density	$\frac{d[X_V]}{dt} = (\mu - k_d)X_V - \frac{(F_{in} - F_{harvest})}{V}X_V$	(17)
Glucose concentration	$\frac{d[GLC]}{dt} = (GLC_{in} - GLC)\frac{F_{in}}{V} - q_{GLC}X_V$	(18)
Glutamine concentration	$\frac{d[GLN]}{dt} = (GLN_{in} - GLN)\frac{F_{in}}{V} - q_{GLN}X_V$	(19)
Lactate concentration	$\frac{d[LAC]}{dt} = q_{LAC}X_V - \frac{F_{in}}{V}LAC$	(20)
Ammonia concentration	$\frac{d[AMM]}{dt} = q_{AMM}X_V - \frac{F_{in}}{V}AMM$	(21)
mAb concentration	$\frac{d[mAb]}{dt} = q_{mAb}X_V - \frac{F_{in}}{V}mAb$	(22)

The typical start-up procedure for the perfusion mode reactor is to operate it as a seeded batch reactor (Banik and Heath, 1995); this initial phase has been disregarded here, as the focus of our study is to perform dynamic optimisation with a view to technoeconomic bioreactor evaluation for extended operation. Other recent studies into bioreactor design (Karst et al., 2017; Shirahata et al., 2019) have similarly not considered the seeding procedure, thus we focus on the main (steady-state) phase therein.

2.4 Generalised dynamic optimisation problem statement

Mathematical optimisation is commonly applied to formulate reactor operating strategies which lead to increased productivity (Biegler, 2010). In these problems, an optimal control strategy is proposed where a system of state variables $\boldsymbol{x}(t)$ is influenced by any number of control (manipulated) variables $\boldsymbol{u}$ so that the control vector $\boldsymbol{u}(t)$ can be sought to minimise (or maximise) an objective variable within the problem. A generic optimisation problem can be seen below in Table 5, this objective is sought to be minimised at the terminal time t_f. The ordinary differential equations for the state variables seen in Eq. (24) are influenced by the control vector $\boldsymbol{u}(t)$ throughout the time domain considered. The initial conditions for the state variables are stated in Eq. (25), whilst constraints across the entire time horizon are considered in Eq. (26). Equality and inequality constraints at the final time are considered in Eq. (27). Finally, the control and state variable boundaries are set in Eq. (28) and Eq. (29).

Table 5: A generalised optimisation problem.

$\min_{\boldsymbol{u}(t),t_f} \varphi(\boldsymbol{x}(t_f), t_f)$	(23)
s.t. $\frac{d\boldsymbol{x}(t)}{dt} = f(\boldsymbol{x}(t), \boldsymbol{u}(t))$	(24)
$\boldsymbol{x}(t_0) = \boldsymbol{x}_0$	(25)
$h(\boldsymbol{x}(t), \boldsymbol{u}(t)) = 0, g(\boldsymbol{x}(t), \boldsymbol{u}(t)) \leq 0$	(26)
$h_f\left(\boldsymbol{x}(t_f)\right) = 0, g_f\left(\boldsymbol{x}(t_f)\right) \leq 0$	(27)
$\boldsymbol{u}(t)_L \leq \boldsymbol{u}(t) \leq \boldsymbol{u}(t)_U$	(28)
$\boldsymbol{x}(t)_L \leq \boldsymbol{x}(t) \leq \boldsymbol{x}(t)_U$	(29)

2.5 Dynamic optimisation solution strategy

A number of methodologies exist to solve optimal control trajectory problems, these include variation methods and finite approximation methods (Biegler, 2010). An example the former is the Euler-Lagrange Multiplier Theorem which applied to single constraint problems (Smith, 1998), whilst the latter represents the control profile using predefined functional forms (Zienkiewicz et al., 2006). For problems with few constraints and decision variables a finite method with sequential strategy is often selected (Buchi et al., 1990). The sequential strategy involves the discretization of the control profile within the system of equations and requires regular re-integration to compute the corresponding state variables (Del Moral et al., 2012). An alternative strategy to this is the simultaneous finite method strategy, which requires the ODE system to be discretized along the time horizon (domain) leading to a NLP problem being formed. The NLP problem can then be tackled using orthogonal collocation techniques (Kameswaran and Biegler 2006; Biegler, 2010). The simultaneous strategy holds the benefits of being faster to solve and better at dealing with larger number of decision variables and constraints (Biegler, 2007), thus it was selected as the strategy of choice here.

3. Results

3.1 Dynamic simulation of a fed-batch reactor for bio manufacture of mAbs

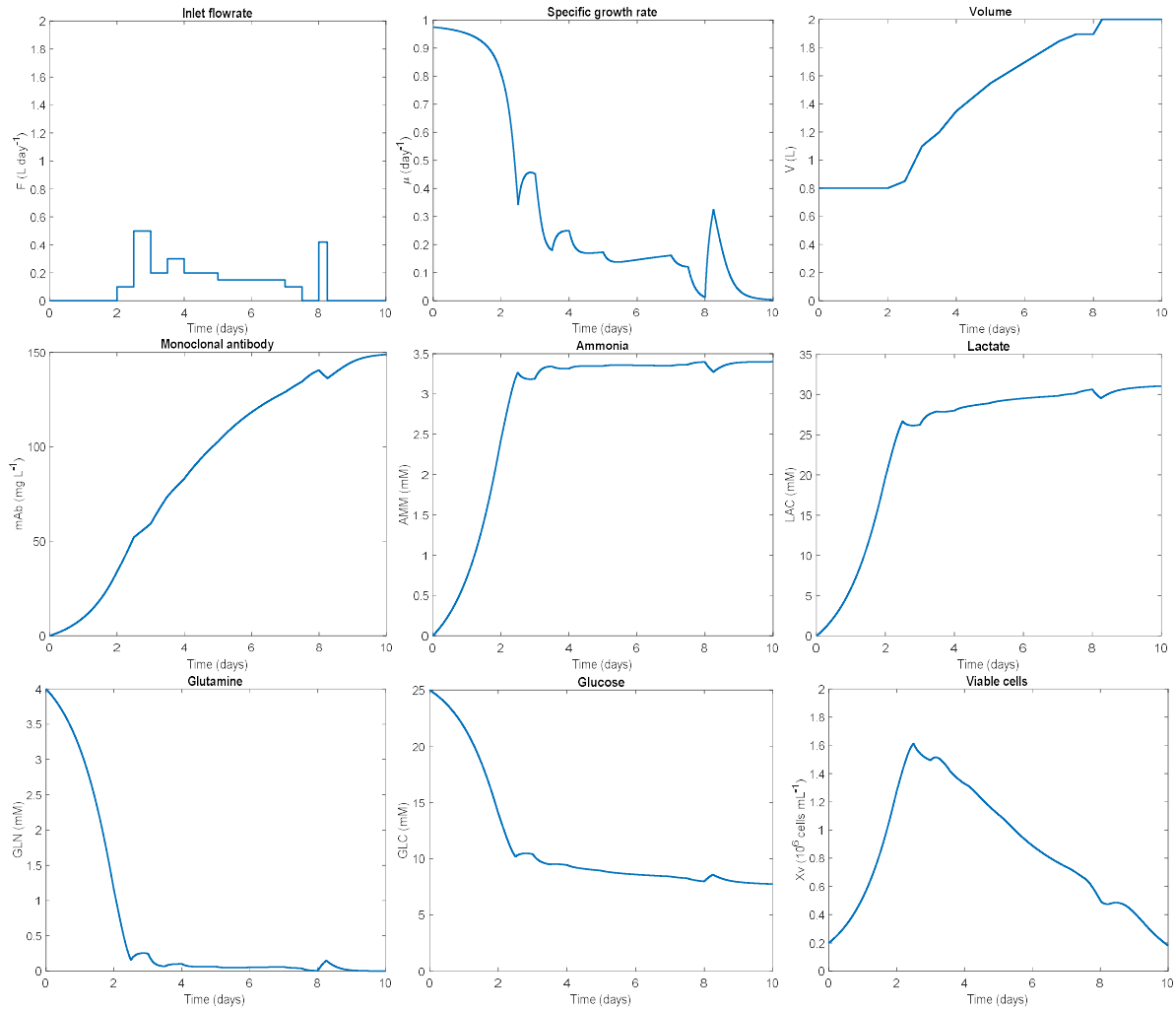

Figure 4: Fed-batch simulation of the hybridoma bioreactions to manufacture mAbs.

Figure 4 displays the trajectories of the model simulation, including the volume, viable cell density and mAb titer, along with other state and intermediate variables of interest. Initial conditions for the fed-batch simulation can be seen in Table 6. The time domain was set at 10 days to allow direct comparison to previous experiments (De Tremblay, et al. 1992). Furthermore, the inlet concentration of the glucose and glutamine were 25mM and 4mM respectively, in-line with the values seen in (De Tremblay, et al., 1992). The simulation applied here was the feeding scheme seen in De Tremblay et al., 1992, it led to a final volume of 2 L and a final mAb titer of 148.951 mg L^{-1}.

Table 6: Initial conditions used for the dynamic simulations

State variables	V_o	$X_{V,0}$	$[GLC]_0$	$[GLN]_0$	$[LAC]_0$	$[AMM]_0$	$[mAb]_0$
Initial condition	0.8 L	$0.2 \cdot 10^6$ cell mL^{-1}	25 mM	4 mM	0 mM	0 mM	0 mM

3.2 Dynamic simulation of a perfusion reactor for bio manufacture of mAbs

Figure 5 displays the results of the model simulation for the perfusion reaction. The same variables seen in Figure 4 are sub-plotted here. The initial conditions for the perfusion simulation were kept identical to those used for fed-batch (Table 6). Again, the time domain (10 days) was kept identical to that of the fed-batch simulation, whilst the harvest flowrate was set to remove half the reactor volume per day. To maintain consistency with the fed-batch simulation, the inlet concentrations here were held at 25mM and 4mM for glucose and glutamine respectively. The feeding, harvest and bleeding strategy for the simulation was taken from the study by (Karst et al., 2017), who looked into how different operating control strategies could be implemented in order to improve the quality of mAb glycan throughputs from perfusion bioreactors.

For operational simplicity the flowrate into the reactor was set equal to the total flowrate out of the reactor, meaning the volume of the reactor and the viable cell density remained constant throughout the time domain (Lindskog, 2018).

The final steady state product concentration was achieved at around day 4, meaning the final 6 days of the experiment led to next to no notable change in the state variable trajectories. For the perfusion simulation, the final mAb titer was 3.920 mg L^{-1}, for a reaction volume of 0.8 L. The total volume added to the reactor from the continuous feed was 11.710 L.

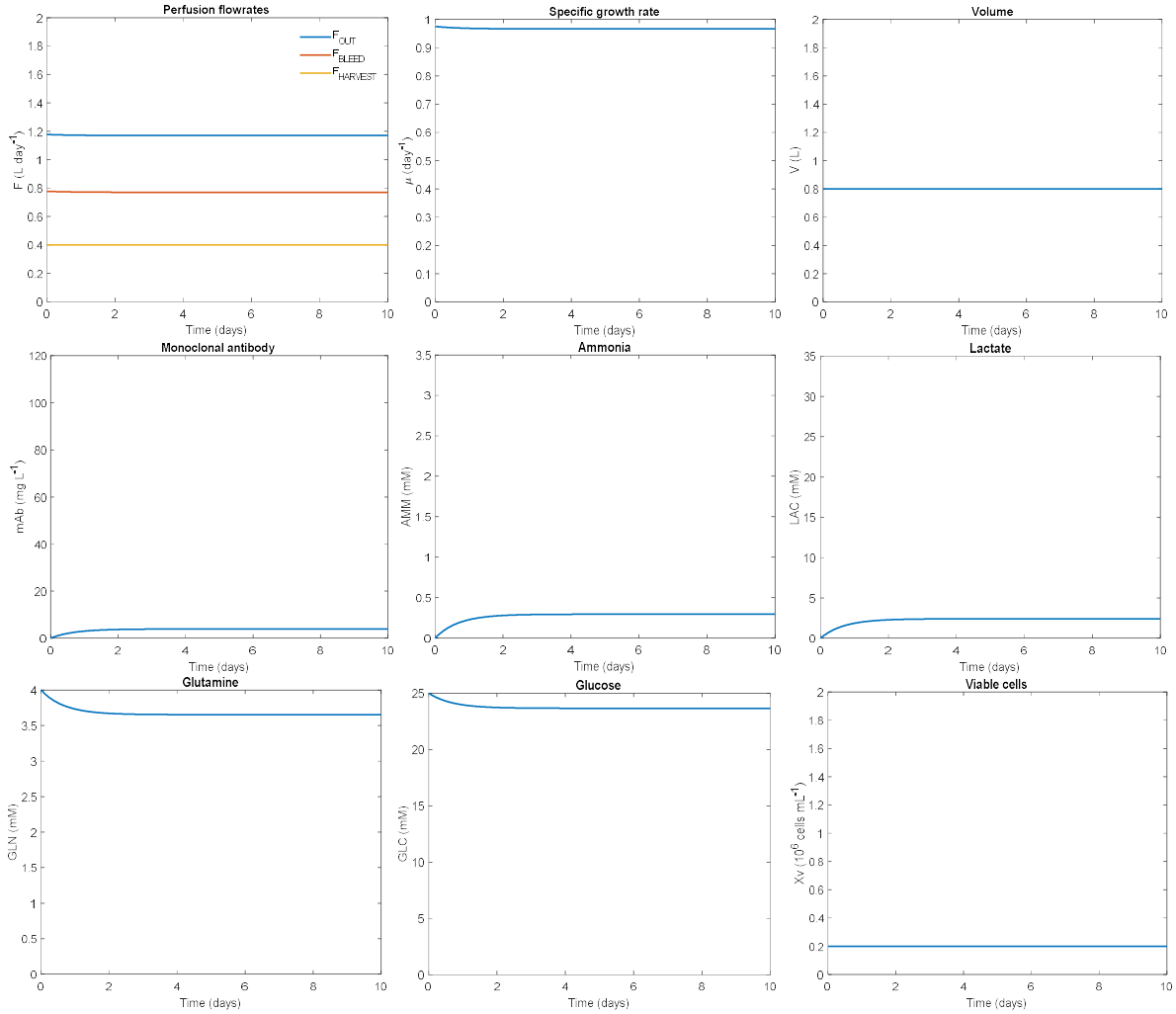

Figure 5: Perfusion simulation of the hybridoma bioreactions to manufacture mAbs.

3.3 Dynamic optimisation of the fed-batch reactor for bio manufacture of mAbs

The software library APOPT was used in a MATLAB 2020b environment so that the control and state variable trajectories could be computed. APOPT can be applied to solve for non-linear programming NLP problems with discretized data points, which is established for the feeding strategy of fed-batch reactor.

In order to optimise for large scale operation of the fed-batch design a reputable source was used to provide a benchmark for the reactor volume. Farid (2007) states that industrial mAb bioreactors typically have working volumes between 10,000 – 20,000 L. Acknowledging this, our design assumed an upper working volume constraint of 12,000 L, whilst the initial volume was set to 75% of this volume constraint, thus 9,600 L. The objective function of the problem was to maximise the final mAb mass within the reactor. The time domain between the changes in inlet flowrate set points was specified as 0.5 days. There were 10 set points for the inlet flowrate, each set point interval was 100 L day^{-1}, meaning the entire inlet flow set point ranged from 0 – 1,000 L day^{-1}.

In this analysis, initial cellular density and reactor campaign length were varied in order to analyse their effects on reactor performance. Four different optimised designs were computed here, each of which were considered candidates for the industrial scale economic analysis. Operating conditions for the four optimised designs have been summarised below in Table 7.

Table 7: Operating conditions for the four optimised fed-batch bioreactor designs.

Experiment	Code	Initial cell density (10^6 cell mL^{-1})	Campaign Length (days)
1	FB-02-15	0.2	15
2	FB-02-30	0.2	30
3	FB-40-15	40	15
4	FB-40-30	40	30

The dynamic optimisation problem for experiment FB-02-15 can be seen in Table 8. In this instance, a single control variable, $F_{in}(t)$ was used as a basis to compute the optimal feeding strategy for improved mAb production. Dynamic optimisation outputs for the experiments FB-02-30 and FB-02-30 can be seen in Figure 6, whilst Figure 7 displays optimisation results for experiments FB-40-15 and FB-40-30.

Table 8: A summary of the fed-batch reactor dynamic optimisation problem for FB-02-15.

Objective function:	$\max_{\boldsymbol{u}(t), t_f = 15 \text{ days}} ([mAb](t = t_f) \cdot V(t = t_f))$
s.t:	
The process model:	$X_i = f_i(X_j(t), \boldsymbol{u}(t), t) \qquad i, j = 1 \dots 6$
The set of inequality constraints:	$9{,}600 \text{ L} \leq V \leq 12{,}000 \text{ L}$
The control vector:	$\boldsymbol{u}(t) = [F_{in}(t)]$ with $0 \text{ L day}^{-1} \leq F_{in} \leq 1{,}000 \text{ L day}^{-1}$
The set of initial conditions:	$V_0 = 9{,}600 \text{ L}$ $X_{V,0} = 0.2 \times 10^6 \text{ cells mL}^{-1}$ $[GLC]_0 = 25 \times 10^{-3} \text{ M}$ $[GLN]_0 = 4 \times 10^{-3} \text{ M}$ $[mAb]_0 = [AMM]_0 = [LAC]_0 = 0 \text{ M}$

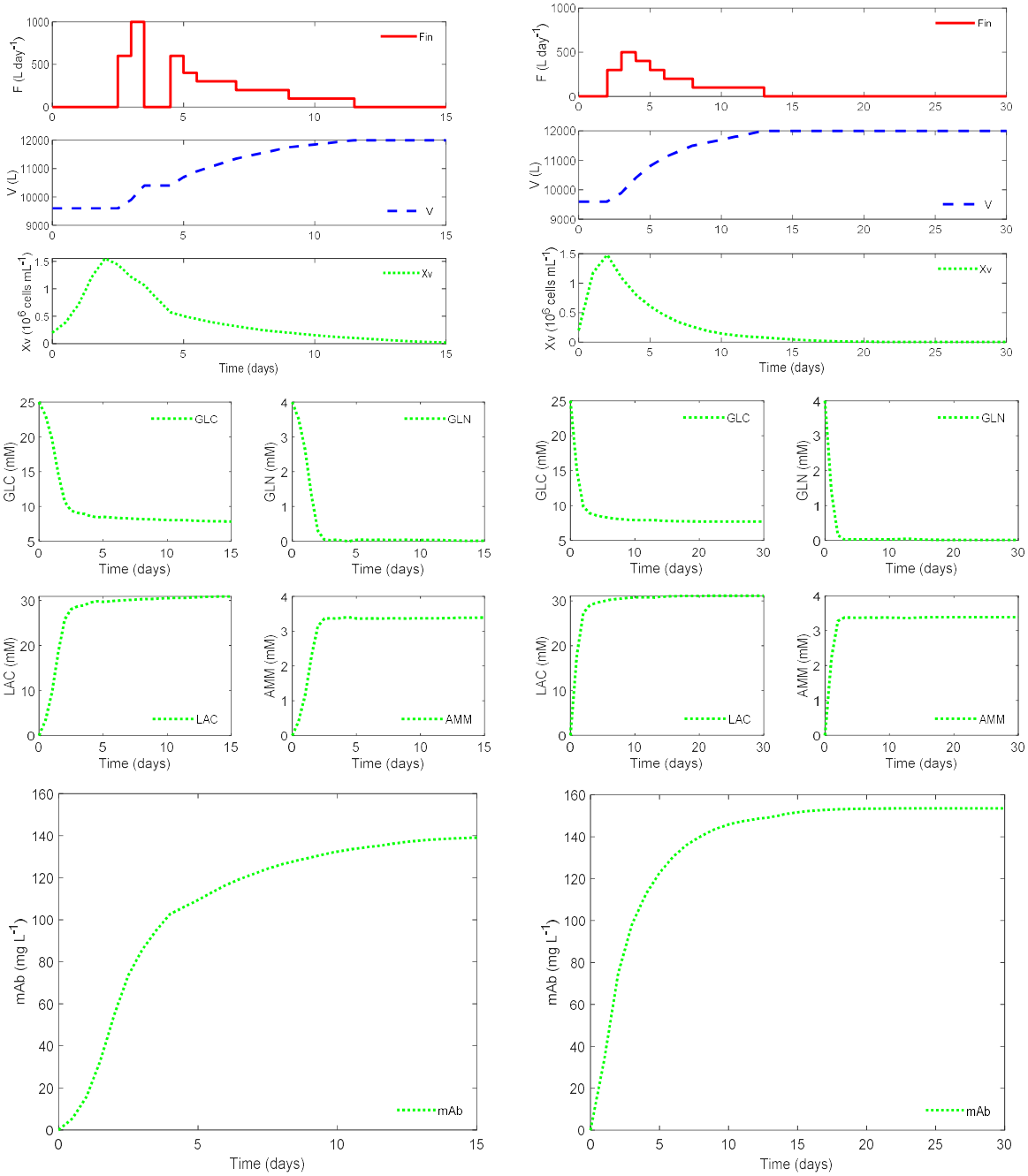

Figure 6: Dynamic optimisation of the fed-batch reactor for FB-02-15 (left) and FB-02-30 (right).

Low cell density designs (FB-02-15 and FB-02-30) exhibited significant growth in viable cell concentration before peaking at around t = 2 days and subsequently diminishing towards $X_V = 0{\cdot}10^6$ cell L^{-1}. This observation is in general agreement with literature on hybridoma cell apoptosis (Balcarcel and Stephanopoulos, 2001). Extended campaign time was shown to be notably beneficial to bioreactor performance; the final titers for the FB-02-15 and FB-02-30 designs were 139.085 mg L^{-1} and 153.607 mg L^{-1} respectively, resulting in total mAb masses of 1.669 kg and 1.843 kg respectively.

In all four fed-batch optimisation trajectories, the final volume settled at the upper limit constraint of 12,000 L, however the period in which upper volume constraint was achieved varied significantly between different experiments. High cell density designs (FB-40-15 and FB-40-30) both achieved the upper volume limit just after t = 5 days, whilst FB-02-15 and FB-02-30 achieved the upper volume limit at approximately t = 12 days.

The rapid feeding strategies seen in the higher cell density designs is attributed to the significantly greater substrate contribution required to avoid early onset massive cell death. Despite the much greater supply of substrates in the early stages of FB-40-15 and FB-40-30 designs, the designs do not exhibit any cell growth, i.e. viable cell density merely decreases from its initial condition. This observation, along with the rapid depletion of glucose and glutamine suggests productivity could be further enhanced via manipulating the concentration of the inlet substrates.

Interestingly, increasing the campaign length only induced a marginal boost to mAb productivity since the final mAb titers were 697.57 mg L^{-1} and 699.22 mg L^{-1} for FB-40-15 and FB-40-30 respectively. The total mAb production for FB-40-15 and FB-40-30 was 8.371 kg and 8.391 kg respectively.

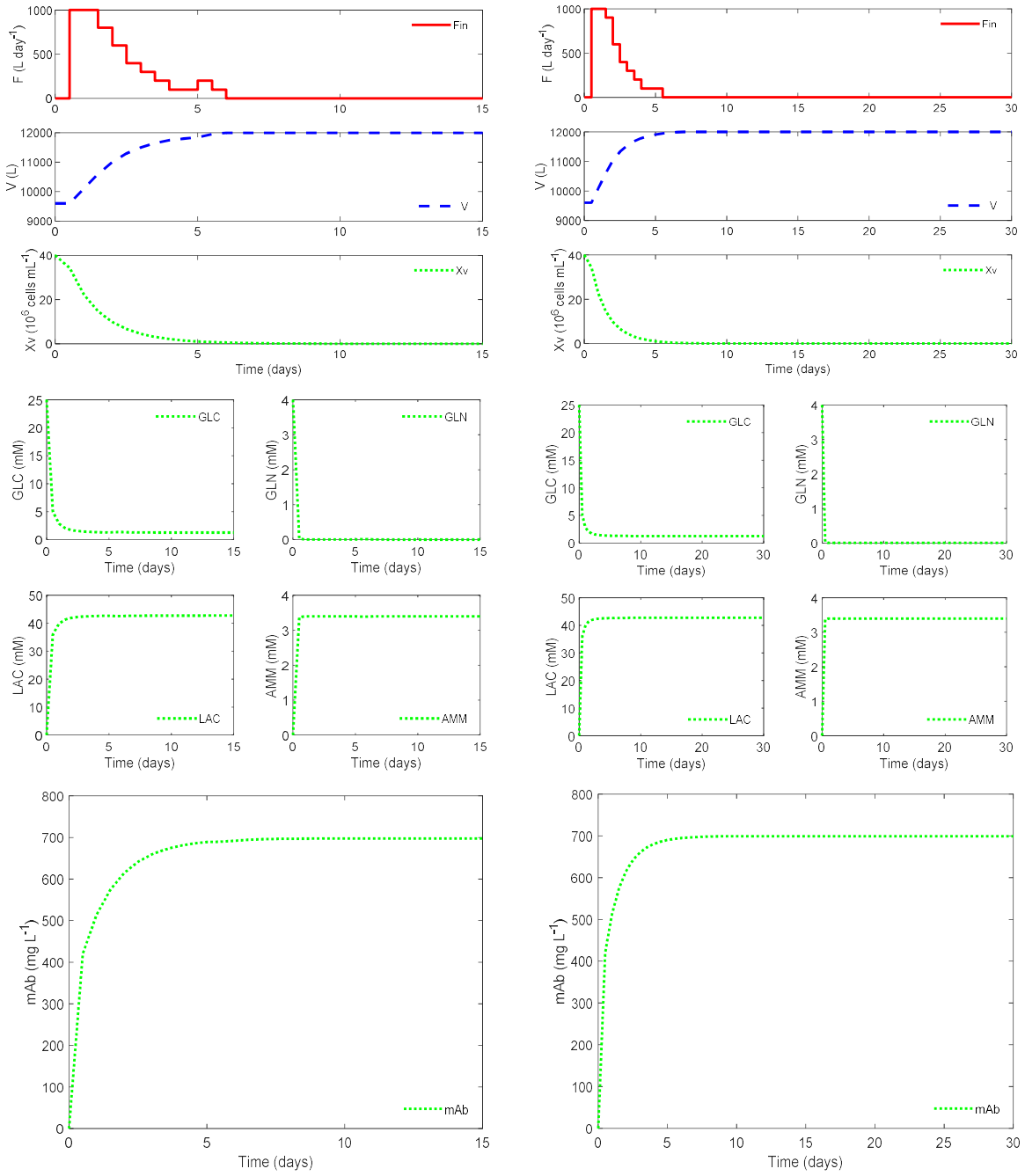

Figure 7: Dynamic optimisation of the fed-batch reactor for FB-40-15 (left) and FB-40-30 (right).

3.4 Dynamic optimisation of the perfusion reactor for bio manufacture of mAbs

The software library IPOPT was applied in a MATLAB 2020b environment to compute the control and state variable trajectories for the perfusion reactor. A key note to make here is there were three manipulated variables $(F_{in}(t),\ F_{harve}\ \ (t),\ F_{bleed}(t))$ for the perfusion optimisation problems compared to one in the previous section for fed-batch optimisation. In order to keep consistency between the fed-batch and perfusion optimisation problems, the manipulated flowrate upper and lower constraints were maintained here from the fed-batch problem. As with the fed-batch designs, 4 designs with variable initial cell densities and campaign lengths were computed for optimised mAb production, the operating conditions of which can be seen in Table 9. Experiment code P-02-15 following an optimal feeding and harvesting strategy was calculated from the dynamic optimisation problem in Table 10.

Table 9: Operating conditions for the four optimised perfusion bioreactor designs.

Experiment	Code	Initial cell density (10^6 cell mL^{-1})	Campaign Length (days)
1	P-02-15	0.2	15
2	P-02-30	0.2	30
3	P-40-15	40	15
4	P-40-30	40	30

The objective function of the problem was to maximise the total mAb mass flowing out of the reactor across the entire time domain. In the case of the perfusion designs, the pre-determined volume for the perfusion reactor designs was set to 2,000 L since this value is cited as the upper boundary for industrial scale perfusion reactors (Bunnak et al., 2016). As with the dynamic simulation, the medium volume remained fixed to its initial value in order to abide by traditional perfusion bioreactor operating standards (Lindskog, 2018).

Figure 8 details the low cell density designs (P-02-15 and P-02-30), whilst Figure 9 details the high cell density designs (P-40-15 and P-40-30). In all four designs, the three manipulated flowrates instantaneously reached their set points and remained there for the entire time domains. Specifically, inlet and harvest flowrates remain fixed at 1000 L day^{-1}, whilst bleed flowrate remained fixed at 0 L day^{-1}. This control strategy is deduced to be optimal for two reasons. Firstly, maintaining a very high harvest flowrate ensures the designs are less prone to an accumulation of culture inhibitors (ammonia and lactate), which would otherwise lead to critical levels of apoptosis. Secondly, bleed flow should only be increased if it beneficial to cell viability, thus in the instance where harmful inhibitors are being harvested it would be best to maintain low levels of bleeding and retain cells within the reactor vessels.

Table 10: A summary of the perfusion reactor dynamic optimisation problem for P-02-15.

Objective function:	$\max_{\boldsymbol{u}(t),t_f=15\text{ days}} \int_0^{t_f} [mAb](t)\cdot F_{out}(t)\ dt$
s.t:	
The process model:	$X_i = f_i(X_j(t),\boldsymbol{u}(t),t) \qquad i,j = 1 \dots 6$
The set of equality constraints:	$V = V_0 = 2{,}000$ L
The control vector:	$\boldsymbol{u}(t) = [F_{in}(t), F_{harvest}(t), F_{bleed}(t)]$ with 0 L day^{-1} $\leq F_{in} \leq$ 1000 L day^{-1}, 0 L day^{-1} $\leq F_{harvest} \leq$ 1000 L day^{-1}, 0 L day^{-1} $\leq F_{bleed} \leq$ 1000 L day^{-1}
The set of initial conditions:	$V_0 = 2{,}000$ L $X_{V,0} = 0.2 \times 10^6$ cells mL^{-1} $[GLC]_0 = 25 \times 10^{-3}$ M $[GLN]_0 = 4 \times 10^{-3}$ M $[mAb]_0 = [AMM]_0 = [LAC]_0 = 0$ M

Low cellular density designs (P-02-15 and P-02-30) both exhibited initial cellular growth, which gradually plateaued at around t = 12 - 15 days. This is distinctly different to the corresponding FB-02-15 and FB-02-30 fed-batch designs, since they both displayed massive cell death once they achieved their peak viable cell concentrations. The ability to maintain viable cell density proves a significant benefit to the productivity of the low cell density systems; the total mAb mass produced for the P-02-15 and P-02-30 designs was 2.442 kg and 5.479 kg respectively, compared to the corresponding FB-02-15 and FB-02-30 designs which produced 1.669 kg and 1.843 kg respectively.

Extension of the campaign length between the low cell density designs (from P-02-15 to P-02-30) appears to not benefit the mAb nor viable cell density trajectories, since steady state operation is achieves at around t = 12 - 15 days. Following the time where steady state operation is reached, the rate of mAb product being harvested remains approximately constant. Therefore, the total mAb extracted from the design is roughly directly proportional to the campaign length of operation.

Just like in the case of the high cell density fed-batch designs, the perfusion control strategy is unable to establish any culture growth from the initial value of $40 \cdot 10^6$ cell L^{-1}. Both P-40-15 and P-40-30 viable cell trajectories decrease from the beginning of the time domain, however, unlike the corresponding fed-batch designs both reach a set point greater than $X_V(t = t_f) = 0 \cdot 10^6$ cell L^{-1}.

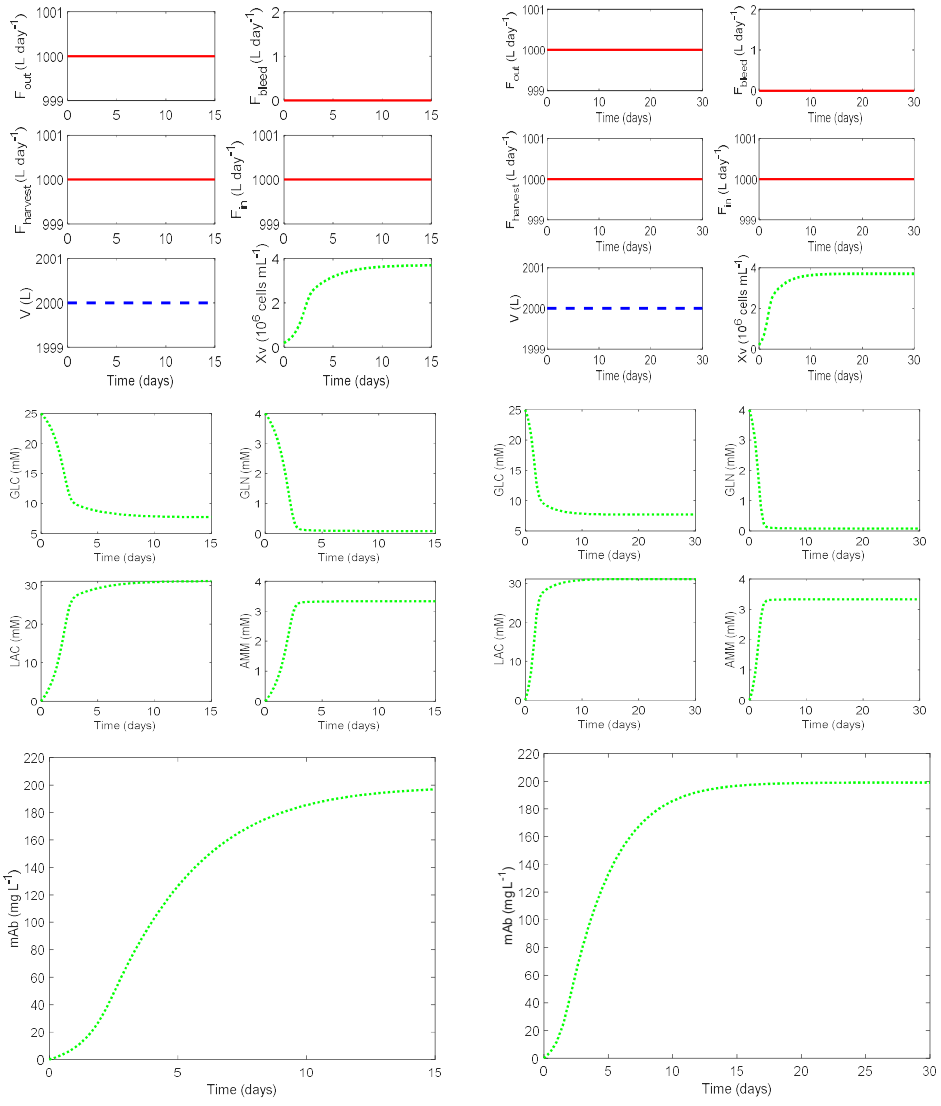

Figure 8: Dynamic optimisation of the perfusion reactor for P-02-15 (left) and P-02-30 (right).

As with the low initial viable cell density perfusion designs, P-40-15 and P-40-30 achieved a steady state mAb and viable cell density trajectory. One thing of note here is the final steady state set points for the low cell density and high cell density designs converged to approximately the same values, this can be attributed to the identical control strategies that were applied across all four designs.

Both P-40-15 and P-40-30 designs exhibited early peaks in mAb titer of 531.3 mg L^{-1} before gradually decreasing to steady state. Prior to this peak in mAb titer the viable cell density was large enough to produce mAb proteins at a faster rate than what was being harvested out of the reactor. Following the peak of mAb production, the combination of massive cell death and declining cellular productivity meant the rate of mAb harvest was greater than mAb production, thus the titer value decreases until the point where production and harvest is equal to one another and steady state is achieved.

Total mAb produced for the P-40-15 and P-40-30 designs was 5.258 kg and 8.660 kg respectively, again showing the importance of campaign length to the performance of these perfusion designs. Despite the improvement compared to the low cell density perfusion designs, P-40-15 was comfortably outperformed by its counterpart FB-40-15, whilst P-40-30 produced a marginally greater mAb mass than its corresponding design FB-40-30.

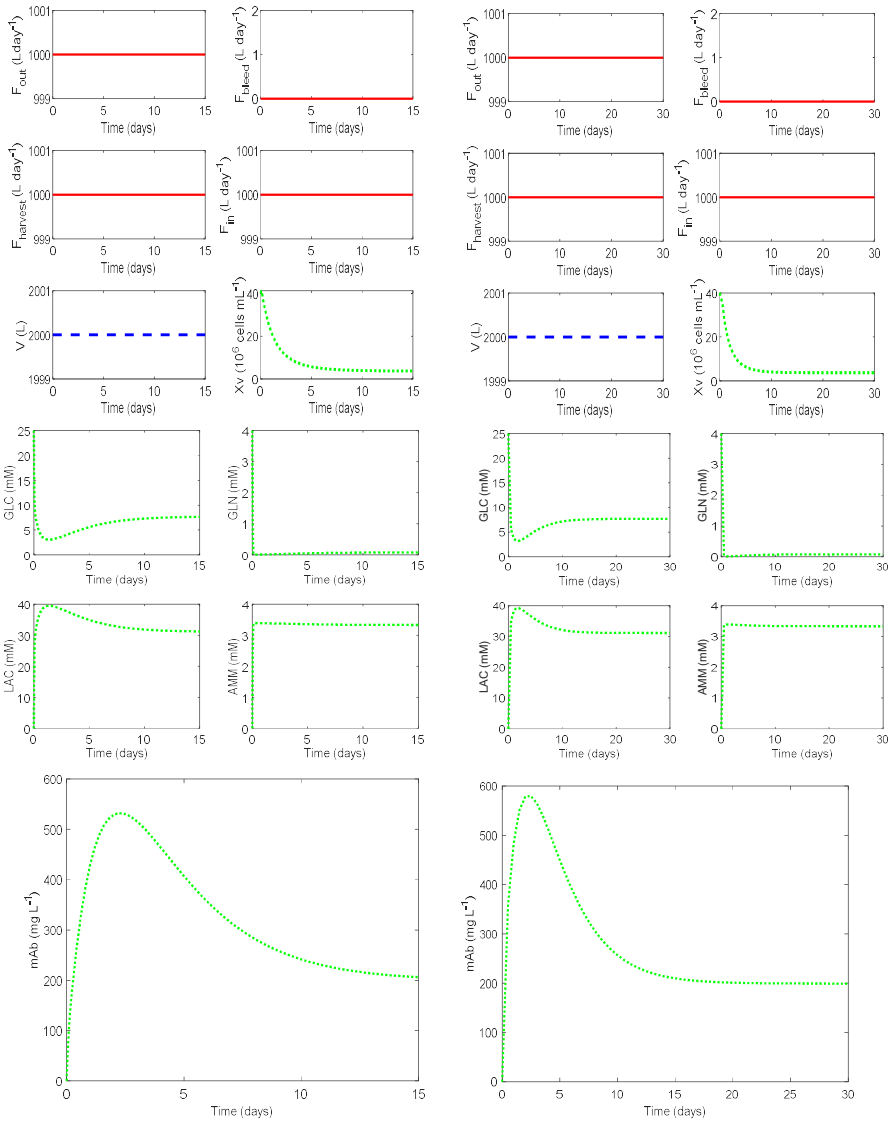

Figure 9: Dynamic optimisation of the perfusion reactor for P-40-15 (left) and P-40-30 (right).

3.5 Material balances of the optimised reactors for mAb bio manufacture

It was necessary to conduct complete material balances of both the fed-batch and perfusion optimised designs in order to fully understand the consequences of each operation. A number of equations were applied to quantify the initial, final, fed, outlet and generation values for the state variables of interest.

The final material quantities were calculated to be the product of final concentration and the final medium volume, this can be computed via the following expression, Eq. (30).

$$M_f = [M]_f \cdot V_f \tag{30}$$

Conversely, initial material quantities were computed as the product of the initial concentration and the initial medium volume, this can be computed via the equation, Eq. (31), below.

$$M_i = [M]_i \cdot V_i \tag{31}$$

Mass fed to the reactor was taken as the integral of the concentration being fed multiplied by the medium flowrate. Consequently, the total masses fed to the reactor throughout the time domains can be computed via the following expression, Eq. (32).

$$M_F = \int_{t_i}^{t_f} [M]_{in}(t) \cdot F_{in}(t)\, dt \tag{32}$$

Outlet mass can be computed as the integral of the material concentration in the reactor multiplied by the reactor outlet flow. The total mass having left the perfusion reactor throughout the time domain can be calculated via the expression below, Eq. (33).

$$M_O = \int_{t_i}^{t_f} [M](t) \cdot F_{out}(t)\, dt \tag{33}$$

The generation terms vary dependent on the state variable being considered. The viable cell generation is defined as integral of the culture growth term seen in the viable cell state variable. This expression can be seen below in Eq. (34).

$$X_{V,G} = \int_{t_i}^{t_f} (\mu - k_d) V[X_V]\, dt \tag{34}$$

In the case of lactate, ammonia and mAb, the total generation within the reactor can be found by formulating the integral of the generation terms within the ODE systems. These expressions for lactate, ammonia and mAb can be seen below in Eq. (35), Eq. (36) and Eq. (37) respectively.

$$LAC_G = \int_{t_i}^{t_f} q_{LAC} V[X_V]\, dt \tag{35}$$

$$AMM_G = \int_{t_i}^{t_f} q_{AMM} V[X_V]\, dt \tag{36}$$

$$mAb_G = \int_{t_i}^{t_f} q_{mAb} V[X_V]\, dt \tag{37}$$

Lastly, glucose and glutamine consumption considers the specific rates of consumption parameters. The total consumption rates for glucose and glutamine is formulated below, in Eq. (38) and Eq. (39).

$$GLC_C = \int_{t_i}^{t_f} q_{GLC} V[X_V]\, dt \tag{38}$$

$$GLN_C = \int_{t_i}^{t_f} q_{GLN} V[X_V]\, dt \tag{39}$$

From applying the expressions seen in this sub section with the optimised trajectories for the fed-batch and perfusion designs, complete material balances for both sets of designs were formulated. All masses here were taken using a kg/batch unit, whilst medium volume and viable cells units were taken as litres and (10^6) cells respectively.

$$M_{kg,i} = \frac{M_{mol,i} \cdot \mathbf{M_i}}{10^3} \tag{40}$$

In order to convert the molar material outputs for glucose, glutamine, lactate and ammonia into kilograms, Eq. (40) was implemented with the molar masses for each component seen in Table 11.

Table 11: Molar mass of ammonia, galactose and manganese.

Molar masses	g/mol	Source
Glucose	180.16	(Kabo et al., 2013)
Glutamine	146.14	(NCBI, 2021a)
Lactate	89.07	(NCBI, 2021b)
Ammonia	17.00	(Pearson, 2008)

Table 12 below represents the flowsheet for the optimised fed-batch and perfusion designs. A select choice of observations from the flowsheet will be highlighted here. Throughout the entire time domain the optimised fed-batch reactors are fed 25% of their initial volumes, whilst the perfusion reactors are fed a remarkable 750% of their initial volumes. Ultimately, this sizeable difference in substrate supply along with the ability to monitor inhibitor (Lactate and Ammonia) concentrations leads to the low viable cell density perfusion designs to outperform the corresponding fed-batch designs. Each perfusion system analysed here was able to produce a net generation in viable cells, thus revealing the importance of the harvest flow in supporting an environment where cell viability is maintained. This is not the case for the optimised fed-batch systems, each of which suffer from net consumption (losses) in viability. The metric of relative viable cell count (RVCC), where final cell count is displayed as relative to the initial cell count can be used to express this phenomena, this term can be found in Eq. (41) below.

$$\text{RVCC}(\%) = \frac{X_{V,0}}{X_{V,t_f}} \times 100 \tag{41}$$

Relative viable cell count of the fed-batch worsened as initial cell density and time domain of reaction both increased. In the instance of the FB-40-15 and FB-40-30 designs, the relative viable cell count is almost negligible (0.00073% and 0.00045% respectively). Despite the FB-02-15 design attaining a significant 13.13% relative viable cell count, this value drops to 0.036% for the FB-02-30 design merely from doubling the reaction time domain. Consequently, the FB-02-30 and FB-40-30 designs exhibit relatively incremental increases in total mAb production compared to their corresponding short term designs, FB-02-15 and FB-40-15 respectively.

Another benefit of the perfusion designs are their consistency in final state variable values for a wide range of operating conditions. For the four operating conditions considered here, each reached steady state before the final time point, meaning the final viable cell mass and mAb mass outputs were both a function of volume only. Conversely, the fed-batch design final state variable values for glucose, lactate and mAb varied significantly when increasing the initial viable cell density condition.

One benefit of the fed-batch designs is the relative total consumption of the substrates is significantly greater than in the perfusion designs. This is particularly prevalent in the long time domain designs, where glutamine is entirely consumed and approximately 93.70% of glucose is consumed in both FB-40-15 and FB-40-30. The high cell density perfusion designs do not achieve complete glutamine consumption (98.30% and 97.54% for P-40-15 and P-40-30 respectively), whilst glucose consumption was a mere 74.48% and 71.79% for P-40-15 and P-40-30 respectively. This considerable difference in consumption of the substrate is partly the cause of the fed-batch design outperforming perfusion for the short time domain with high cell density designs (FB 40-15 and P-40-15).

Table 12: Material balances for the optimised bioreactor designs.

Fed-Batch											
		FB-02-15					FB-02-30				
State	**Units**	**Initial**	**Fed**	**Generated/Consumed**	**Outlet**	**Final**	**Initial**	**Fed**	**Generated/Consumed**	**Outlet**	**Final**
Media	L	9600	2400	0	0	12000	9600	2400	0	0	12000
Viable Cells	(10^6) cells	1920000	0	-1667974	0	252026	1920000	0	-1919309	0	691
Glucose	kg/batch	43.24	10.81	-37.11	0	16.94	43.24	10.81	-37.40	0	16.65
Glutamine	kg/batch	5.61	1.41	-7.00	0	0.02	5.61	1.40	-6.99	0	0.02
Lactate	kg/batch	0	0	33.03	0	33.03	0	0	33.28	0	33.28
Ammonia	kg/batch	0	0	0.69	0	0.69	0	0	0.69	0	0.69
mAb	kg/batch	0	0	1.67	0	1.67	0	0	1.84	0	1.84
		FB-40-15					FB-40-30				
Media	L	9600	2400	0	0	12000	9600	2400	0	0	12000
Viable Cells	(10^6) cells	384000000	0	-383997208	0	2792	384000000	0	-383998256	0	1744
Glucose	kg/batch	43.24	10.81	-51.31	0	2.74	43.24	10.58	-51.11	0	2.71
Glutamine	kg/batch	5.61	1.40	-7.01	0	0.00	5.61	1.37	-6.98	0	0.00
Lactate	kg/batch	0	0	45.66	0	45.66	0	0	45.68	0	45.68
Ammonia	kg/batch	0	0	0.69	0	0.69	0	0	0.69	0	0.69
mAb	kg/batch	0	0	8.37	0	8.37	0	0	8.39	0	8.39
Perfusion											
		P-02-15					P-02-30				
Media	L	2000	15000	0	15000	2000	2000	30000	0	30000	2000
Viable Cells	(10^6) cells	400000	0	52034335	45046675	7387660	400000	0	108584934	1015766	7408270
Glucose	kg/batch	9.01	67.56	-46.26	27.52	2.78	9.01	135.12	-93.75	47.60	2.77
Glutamine	kg/batch	1.17	8.77	-8.78	1.13	0.03	1.17	17.54	-17.51	1.17	0.02
Lactate	kg/batch	0	0	41.17	35.63	5.54	0	0	83.43	77.88	5.55
Ammonia	kg/batch	0	0	0.87	0.75	0.12	0	0	1.73	1.62	0.11
mAb	kg/batch	0	0	2.44	2.05	0.39	0	0	5.48	5.08	0.40
		P-40-15					P-40-30				
Media	L	2000	15000	0	15000	2000	2000	30000	0	30000	2000
Viable Cells	(10^6) cells	80000000	0	43459600	115986505	7473095	80000000	0	111202431	183793717	7408714
Glucose	kg/batch	9.01	67.56	-57.03	16.78	2.75	9.01	135.1	-103.47	37.88	2.77
Glutamine	kg/batch	1.17	8.77	-9.77	0.14	0.02	1.17	17.54	-18.25	0.44	0.02
Lactate	kg/batch	0	0	50.75	45.19	5.57	0	0	92.08	86.53	5.55
Ammonia	kg/batch	0	0	0.97	0.85	0.11	0	0	1.80	1.69	0.11
mAb	kg/batch	0	0	5.26	4.85	0.41	0	0	8.66	8.26	0.40

3.6 Cost analysis of the optimised fed-batch and perfusion reactors for mAb manufacture

The disparity between the material output of mAb product of these designs means careful selection of operating strategies should be considered prior to the economic analysis. It was essential to consider all aspects of economic insight of both systems, whilst also setting a nominal material output as a benchmark to allow for fair and clear comparative analysis.

Both designs were formulated to operate at approximately 8000 operating hours per year. 8000 operating hours enabled annual production of 22 batches per year for the 15 day campaign designs and 11 batches per year for the 30 day campaign designs. The nominal basis for the analysis was selected to be 200 kg/year since this was deemed an appropriate industrial mass output (Klutz et al., 2016).

The cost analysis is split into two subsections, firstly the total capital costs (CapEx) and operating costs (OpEx) for optimised fed-batch and perfusion industrial scale designs were investigated. To account for the industrial scale manufacturing facility, the CapEx consisted of Equipment Purchase Cost (EPC), Total Direct Cost (TDC) and Total Indirect Cost (TIC). The cost values for all these factors were obtained via a combination of vendor prices, reputable literature sources and applying equipment price scaling formulas. Accordingly, the CapEx could be computed below with Eq. (42).

$$\mathrm{CapEx} = \mathrm{EPC} + \mathrm{TDC} + \mathrm{TIC} \tag{42}$$

Alongside CapEx, the operating expenditure (OpEx) must be considered. In this analysis, the necessary raw materials (C_{RM}), utilities (C_U) and waste treatment (C_{WT}) were accounted for. The raw materials consisted of the cell culture and the culture medium, whilst the utilities consisted of electricity (for heating and mixing), water, labour and cleaning chemicals (sodium chloride and nitric acid). All the components for OpEx are cited from vendors and relevant literature references. Consequently, the OpEx for the designs could be computed with Eq. (43).

$$\mathrm{OpEx} = \mathrm{C_{RM}} + \mathrm{C_U} + \mathrm{C_{WT}} \tag{43}$$

The second subsection of the economic analysis attempted to understand the viability of these designs over a considerable plant lifetime. Two metrics were used to investigate these two sets of designs over the time domain considered, namely Net Present Cost (NPC) and the Cost of Goods Sold per gram (COGS). In these two metrics, the value of OpEx was modelled as dynamic in order to account for inflation changes over the plant lifetime. The expression for NPC can be seen below in Eq. (44).

$$\mathrm{NPC} = \mathrm{CapEx} + \sum_{i=1}^{\tau} \left(\frac{\mathrm{OpEx}}{(1-r)^i} \right) \tag{44}$$

In this expression, a 15 year analysis is considered, i.e. $\tau = 15$. The interest rate here is defined as a fixed value of r for the entire 15 years process lifetime, this fixed value was varied in the analysis to elucidate the sensitivity of the optimised designs to market pressures.

Finally, the equation for COGS analysis is detailed in Eq. (45).

$$\mathrm{COGS} = \frac{\mathrm{NPC\ (£)}}{\mathrm{Total\ mAb\ Production\ (g)}} \tag{45}$$

The COGS analysis is dependent on the time point considered, thus COGS was computed at the end of each operating year throughout the plant lifetime.

Table 13 lists the OpEx and CapEx expenses along with the sources where the cost data was obtained. The ATF filter used in the separation of perfusion outlet flow into bleed and harvest flows was costed via the six tenth rule (Green and Southard, 2019), which can be used to estimate cost values for equipment with capacities different to those found in literature. The equation for this expression can be seen below in Eq. (46).

$$C_A = C_B \left(\frac{S_A}{S_B}\right)^{0.6} \tag{46}$$

The culture medium cost consisted of the initial media placed in the vessel, along with any media added to the vessel throughout the time domain, this can be represented by Eq. (47) below.

$$C_{media} = CU_{media}(V_0 + \int_0^{t_f} F_{in}\ dt) \tag{47}$$

Electricity costs accounted for the heating required to maintain the fermenters at a 36.5 °C, along with mixing power required to ensure the concentrations and temperature within the fermenters were uniform. The total electrical power, cost, heating power, Reynolds number and mixing power are formulated in Eq. (48), Eq. (49), Eq. (50), Eq. (51) and Eq. (52) respectively (Welty et al., 2020). The total electricity efficiency was assumed to be 60%.

$$P_{total} = P_{heating} + P_{mixing} \tag{48}$$

$$C_{electrcity} = CU_{electricity} P_{total} \tag{49}$$

$$P_{heating} = \dot{m}_{solution} c_p \Delta T + UA_{vessel} \Delta T \tag{50}$$

$$Re = \frac{ND^2 \rho_{solution}}{\mu_{solution}} \tag{51}$$

$$\begin{aligned} P_{mixing} &= k\mu_{solution} N^2 D^3 \ (10 < Re < 100) \\ P_{mixing} &= N_p \rho_{solution} N^3 D^5 \ (100 \leq Re) \end{aligned} \tag{52}$$

Solution heat capacity, density and viscosity were taken as the corresponding standard conditions for water, i.e. 4.18 kJ kg^{-1} $C^{\circ -1}$, 1,000 kg m^{-3} and 10^{-3} Pa·s respectively (Green and Southard, 2019). The vessel material was assumed to be glass lined stainless steel. Thus based on literature sources, the overall heat transfer coefficient (OHTC) for the design could be approximated to be 250 W m^{-2} K^{-1} (Johnson et al., 2016; Green and Southard, 2019). The agitator used in mixing operated with a stirring speed of $N = 4$ s^{-1}, whilst the parameters N_p and k were dependent on the type of agitator used (Sinnott, 2005; Pinelli, et al. 2010). For both designs, the agitator was assumed to be an angle bladed impeller, thus the N_p could be approximated via power number vs Reynolds number correlations (Sinnott, 2005). Furthermore, the agitator diameter was set to equal 0.7 times the total fermenter diameter. The fermenter dimensions are considered below in Eqs. (53–55).

$$V_F = H \frac{\pi {D_F}^2}{4} \tag{53}$$

$$\frac{H}{D_F} = 3 \tag{54}$$

$$D = 0.7 D_F \tag{55}$$

Table 13: OpEx and CapEx contributions to reactor design.

Operational Expenditure				
Cost component	Description	Value	Cost unit	Source
Raw material	Hybridoma cells	$9.36 \cdot 10^{-4}$	£ cell $^{-1}$ mL	(Badr et al., 2021)
Raw material	Culture medium	0.0048	£ mL $^{-1}$	(Badr et al., 2021)
Utility	Mixing	0.106	£ kWh $^{-1}$	(Han et al., 2016)
Utility	Heating	0.106	£ kWh $^{-1}$	(Han et al., 2016)
Utility	NaCl	2.859	£·L $^{-1}$	(Chemicals, 2021b)
Utility	Nitric Acid	5.912	£·L $^{-1}$	(Chemicals, 2021a)
Utility	Water	0.023	£·L $^{-1}$	(Karagiannis and Soldatos, 2008)
Utility	Labour	16	£ person^{-1} hr^{-1}	(-)
Waste	Waste treatment	0.40	£·L $^{-1}$	(Schaber et al., 2011)
Capital Expenditure				
Equipment Purchase Cost (EPC)				
Cost component	Description	Value	Cost unit	Source
Equipment	Vessel material	6597.54	£ $(L^{-1})^{0.6}$	(Vermasvuori and Hurme, 2011)
Equipment	ATF filter	68763	£ $(m^{-2})^{0.6}$	(Woods, 2007)
Direct/Indirect Cost (TDC/TIC)				
Cost component	Description	Value	Cost unit	Source
Direct	Installation	0.5	£·EPC	(Petrides, 2000)
Direct	Process Piping	0.4	£·EPC	(Petrides, 2000)
Direct	Instrumentation	0.35	£·EPC	(Petrides, 2000)
Direct	Insulation	0.03	£·EPC	(Petrides, 2000)
Direct	Electrical	0.15	£·EPC	(Petrides, 2000)
Direct	Buildings	0.45	£·EPC	(Petrides, 2000)
Direct	Maintenance	0.01	£·EPC	(Vermasvuori and Hurme, 2011)
Indirect	Construction	0.35	£·EPC	(Petrides, 2000)
Indirect	Contingency	0.50	£·EPC	(Han et al., 2016)
Indirect	Contractors Fee	0.05	£·EPC	(Han et al., 2016)

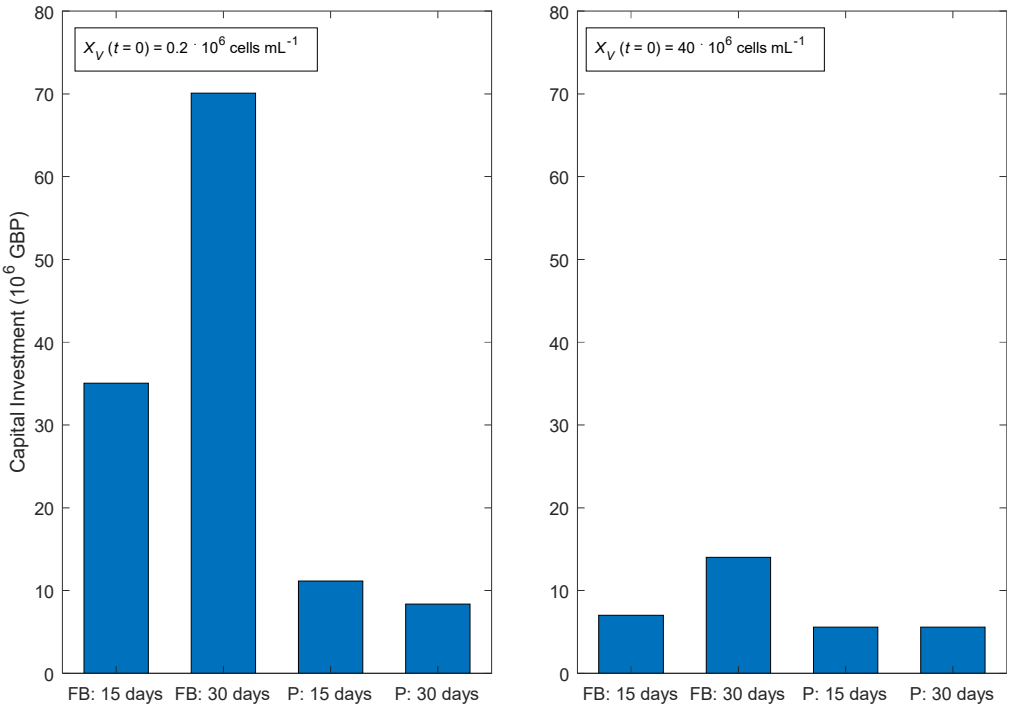

Figure 10: CapEx for the optimised designs.

The Reynolds number for the reactors were calculated to be $1.98 \cdot 10^6$ and $5.80 \cdot 10^6$ for the perfusion and fed-batch designs respectively. This meant both designs attained power number parameter (N_p) values of 1.5 and enabled the second expression in Eq. (52) to be used to formulate mixing power.

Clean-in-place (CIP) strategies detailed within (Bremer et al., 2006) and (Niamsuwan et al., 2011) were used as frameworks for the cleaning schedules for both reactor designs. This meant 1,972 L and 35 L 1% w/v solutions of sodium chloride and nitric acid respectively were used in conjunction with 2,378 L of water to flush the perfusion units at the end of each batch. In the case of the fed-batch designs, 11,834 L and 210 L 1% w/v solutions of sodium chloride and nitric acid respectively were applied with 14,266 L of process water for CIP.

Total capital cost values for the eight designs can be seen in Figure 10. The most prominent observation is the sizeable capital spending needed for the low cell density fed-batch designs, making them very unattractive to investors. The high initial cell density fed-batch designs exhibit greatly reduced CapEx, primarily due to the increased mAb productivity leading to a lower number of reactors needed to achieve the 200 kg/yr annual output. The perfusion design CapEx is significantly lower than the fed-batch designs for low initial cell conditions, and slightly lower than the fed-batch designs for high initial cell conditions. Primarily the differences observed here are due to differences in vessel sizes and mAb productivities. Perfusion designs for P-40-15 and P-40-30 have identical capital expenditures since both require exactly two vessels to meet the annual 200 kg/yr production demand. Consequently, the choice between these two designs would be made entirely from comparing the annual OpEx values and reactor productivities.

Operational expenditure breakdowns for the optimised designs are detailed below in Figure 11. As with the case for CapEx, FB-02-15 and FB-02-30 appear the weakest design options. The much larger vessel sizes contributed to a significant increase in heating and mixture duties compared to the corresponding P-02-15 and P-02-30 designs for perfusion. Furthermore, in the case of low initial cell designs, more fed-batch vessels are needed to reach the nominal mass requirement compared to the perfusion systems; FB-02-15 and FB-02-30 require 5 and 10 vessels respectively whereas P-02-15 and P-02-30 require 4 and 3 vessels respectively. These additional units lead to significant differences in labour demand, especially when comparing FB-02-30 to P-02-30.

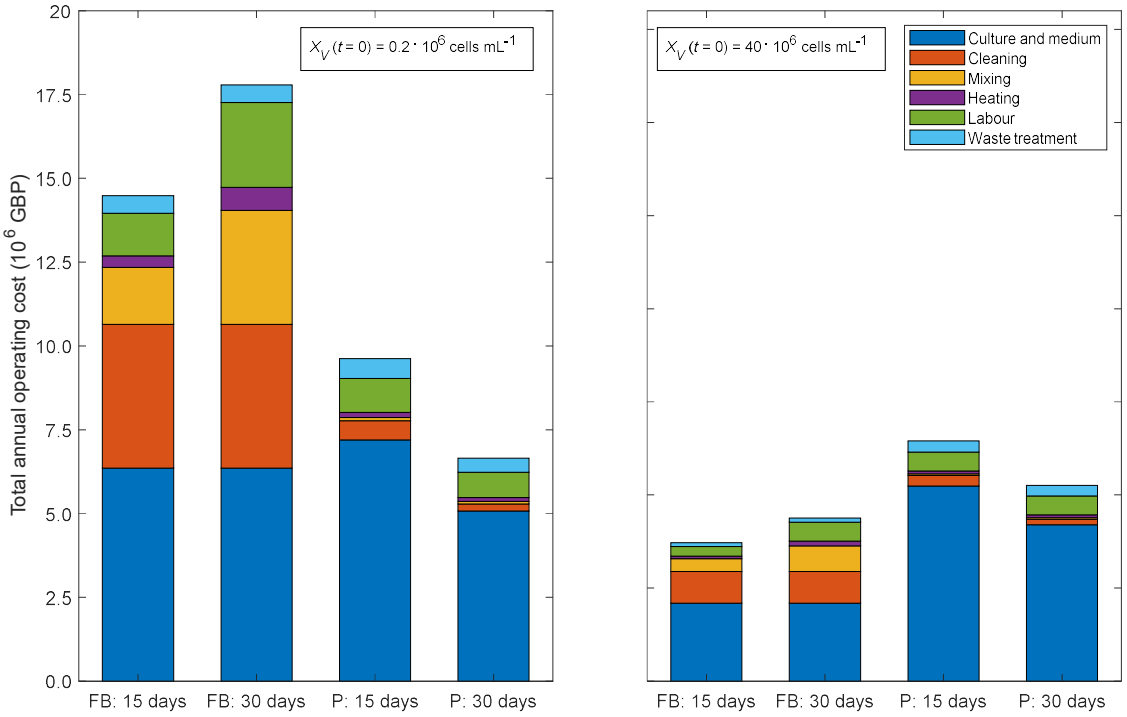

Figure 11: OpEx breakdown for the optimised designs.

High cell density designs for fed-batch (FB-40-15 and FB-40-30) yield the smallest total OpEx values of all the designs considered. This is due to the combination of significant mAb productivity coupled with a restricted usage of medium throughout the time domains. FB-40-15 achieved a slightly lower OpEx than FB-40-30, this is due to the additional vessel needed for FB-40-30 to achieve the annual mAb production basis. FB-40-15 is the only design requiring one vessel to achieve demand; FB-40-30, P-40-15 and P-40-30 all require two. Medium requirements for the P-40-15 and P-40-30 perfusion designs hinder their industrial prospects. Not only is the bulk purchase of the vast quantity of medium harmful but also the considerable waste treatment which results from the medium demand.

As stated previously in the methodology, two metrics were applied in order to evaluate the long term economic outlook for the industrial scale optimised designs, these were the NPC and COGS. This analysis considered a plant lifetime of 15 years, with a fixed interest (inflation) rate, however the value for the interest rate was not pre-determined. Naturally, interest rate is a dynamic parameter which is dependent on market pressures, according to (Musarat et al., 2021), inflation of approximately 2-5% is typical for the global market, with emerging markets shown to be closer to the upper region of that percentage boundary. Since the selection of a fixed interest rate is an arbitrary procedure, it was seen appropriate to test a range of interest rate values here. The range of interest rates analysed were the integers from 1-10%, with the aim of encompassing broad market uncertainty on the economic outlooks of both the optimised fed-batch and perfusion designs. Figure 12 and 14 represent the NPC values and COGS for the industrial scale designs for the range of interest rates.

As with the CapEx and OpEx analysis, the NPC trajectories point to the low cell density condition designs being significantly more expensive across the plant lifetime than corresponding high cellular density designs. Ultimately this analysis supports the notion that for low cell density conditions, a perfusion mode of operation should selected, whilst for high cell density conditions a fed-batch system should be selected.

The COGS plots further established the fed-batch designs inadequacy at operating cost effectively with low initial viable cell densities. At any given interest rate there were no time points in which either FB-02-15 or FB-02-30 achieved a COGS value below £75/g.

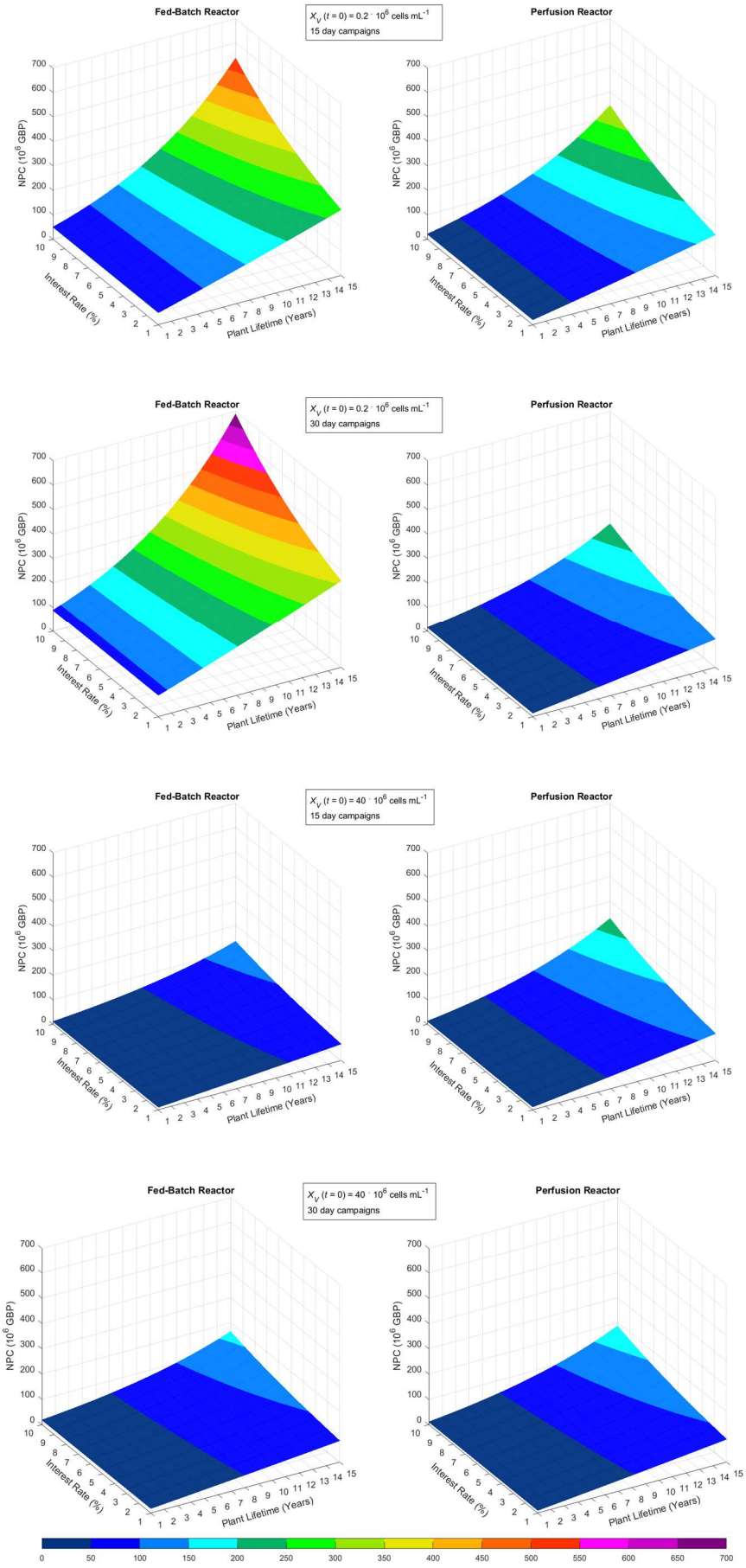

Figure 12: NPC trajectories for the optimised designs.

Furthermore, the significant capital investment needed for FB-02-15 and FB-02-30 designs (5 and 10 reactor vessels are needed respectively) means that the first year COGS values for these designs are £247.60/g and £433.32/g respectively. Whilst it is clear perfusion should be the choice the for the low cell density systems, caution should be considered regarding their long term viability for larger interest rates. Considering the COGS trajectories for P-02-15 and P-02-30, both exhibit significant spikes in value towards the end of plant lifetime for 8-10% interest rates leading to COGS values reaching values greater than they were in year 1. Again, fed-batch appears to outperform perfusion for high cell density designs, however, the level of performance is much more comparable than the low cell density designs. FB-40-15 and FB-40-30 produced COGS values lower than their corresponding perfusion designs (P-40-15 and P-40-30) for the vast majority of time points and interest rates considered. The smallest mean average final COGS value for the eight designs considered is FB-40-15, achieving a value of £34.76/g.

The COGS analysis findings are very important, indicating that fed-batch offers definite cost savings in comparison to perfusion mode. Figure 13 presents COGS values for the FB-40-15, P-40-15, FB-40-30 and P-40-30 (high density) designs, for different interest rates, and a plant lifetime point of 10 years. These results are in excellent agreement with relevant comparison trends published (Badr et al., 2021).

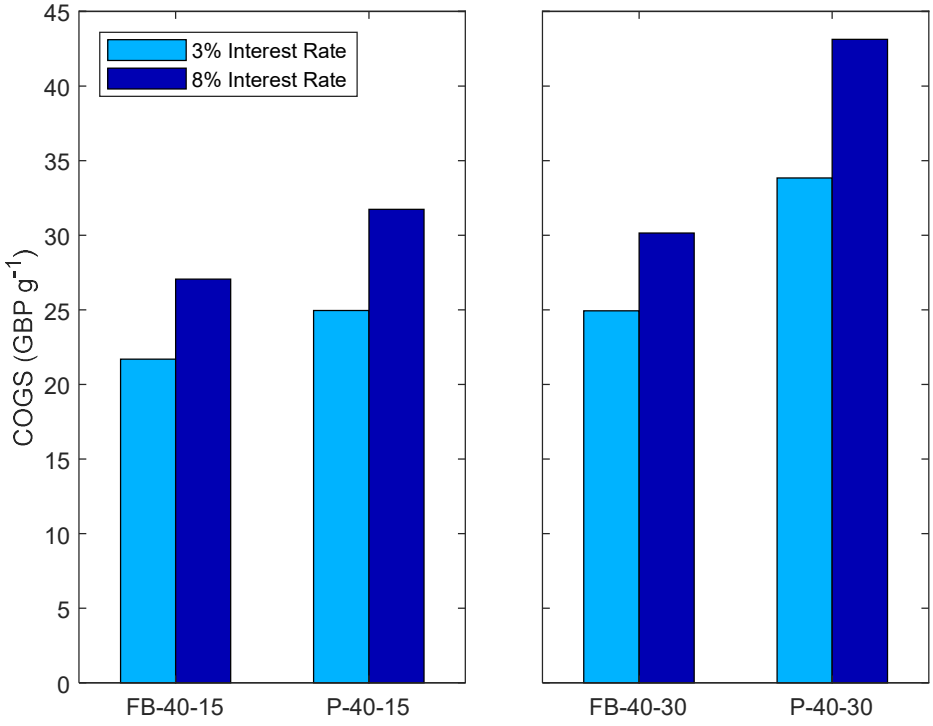

Figure 13: COGS values for the high cell density designs at plant lifetime of 10 years

The comprehensive economic analysis of the two most promising(one fed-batch, one perfusion) designs is presented in Table 14, with a detailed cost breakdown for both CapEx and OpEx (for the first year). FB-40-15 and P-40-15 are the two designs considered, as these two achieve the lowest mean average COGS values over the 15-year plant lifetime. The sizing specification for the optimised fed-batch reactor was taken as the vendor size of vessels used at the Genentech, Vacaville, CA, USA facility, the earliest facility referenced by Farid (2007). With this 12,000 L size fed-batch reactor, a total annual mAb output of 184.16 kg/yr per reactor is established. Of this list of discrete reactor volume values provided by the various vendors (Farid, 2007), 12,000 L is the vendor size which produces an output closest to the annual target of 200 kg/yr. As a result of this, a full economic analysis is provided here on the basis of a 184.16 kg/yr output of mAb from the optimised fed-batch reactor. Table 14 clearly indicates the industrial feasibility of the perfusion design is dependent on its smaller CapEx. The per batch mAb productivity of the P-40-15 is significantly smaller than FB-40-15, meaning 2 reactors are needed to achieve the nominal mass and its per reactor OpEx is somewhat larger than FB-40-15 too.

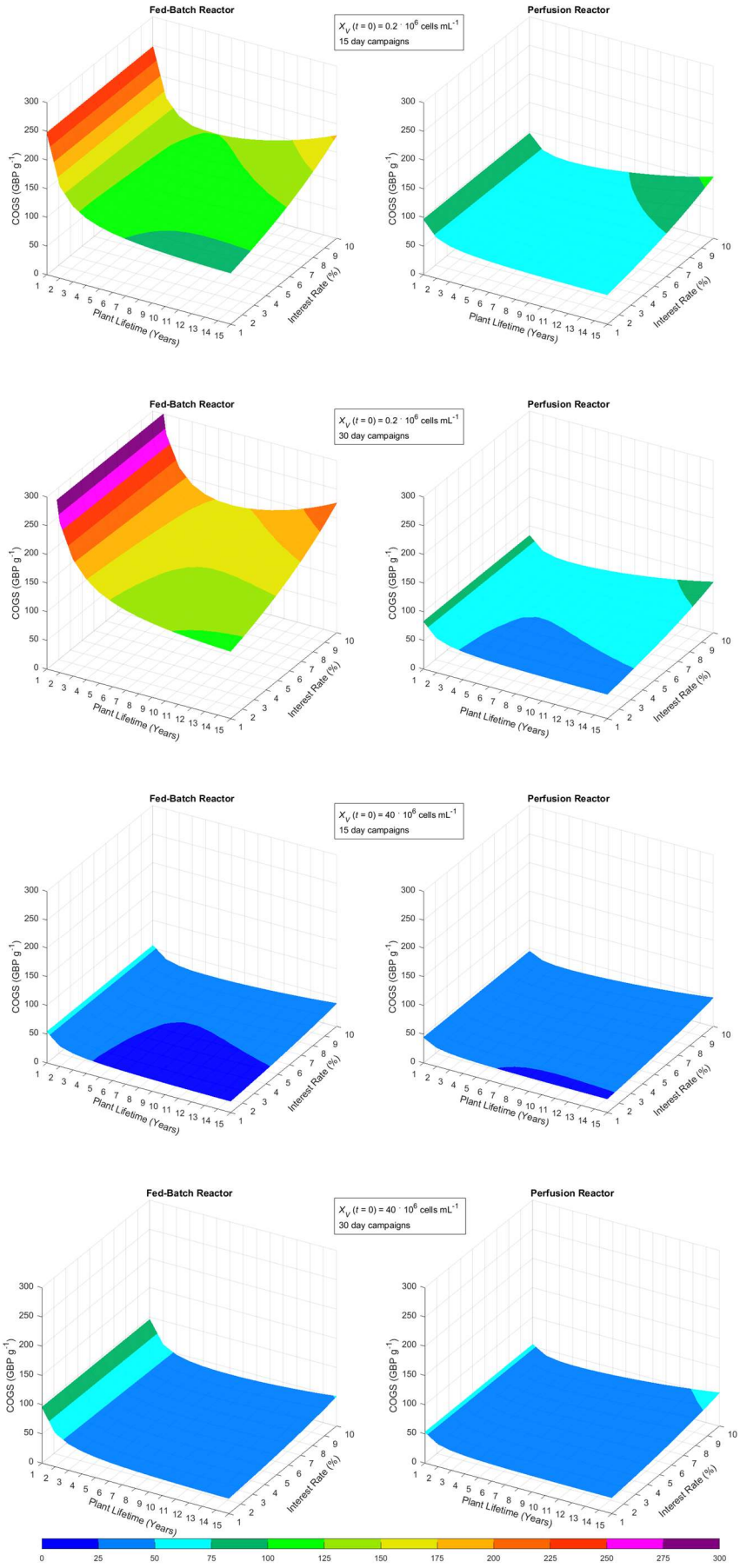

Figure 14: COGS trajectories for the optimised designs.

Table 14: Reactor cost breakdown (first year of operation) for FB-40-15 and P-40-15 designs.

Operational Expenditure							
		Fed-Batch			Perfusion		
Cost component	Description	Quantity	Price	Cost	Quantity	Price	Cost
Raw material	Hybridoma cells	$4.00 \cdot 10^{7}$ cell mL^{-1}	£ $9.36 \cdot 10^{-4}$ cell $^{-1}$ mL	£ 37,440	$4.00 \cdot 10^{7}$ cell mL^{-1}	£ $9.36 \cdot 10^{-4}$ cell $^{-1}$ mL	£ 37,440
Raw material	Culture medium	$1.20 \cdot 10^{7}$ mL	£ 0.0048 mL $^{-1}$	£ 57,600	$1.70 \cdot 10^{7}$ mL	£ 0.0048 mL $^{-1}$	£ 81,600
Utility	Mixing	$1.46 \cdot 10^{5}$ kWh	£ 0.106 kWh $^{-1}$	£ 15,470	$9.98 \cdot 10^{3}$ kWh	£ 0.106 kWh $^{-1}$	£ 1,058
Utility	Heating	$2.99 \cdot 10^{4}$ kWh	£ 0.106 kWh $^{-1}$	£ 3,166	$1.63 \cdot 10^{4}$ kWh	£ 0.106 kWh $^{-1}$	£ 1,732
Utility	Sodium Chloride	$1.18 \cdot 10^{4}$ L	£·2.8592 L $^{-1}$	£ 33,835	$1.97 \cdot 10^{3}$ L	£·2.8592 L $^{-1}$	£ 5,639
Utility	Nitric Acid	$2.10 \cdot 10^{2}$ L	£ 5.912·L $^{-1}$	£ 1,240	$3.50 \cdot 10^{1}$ L	£ 5.912·L $^{-1}$	£ 207
Utility	Water	$1.68 \cdot 10^{5}$ L	£ 0.023 L $^{-1}$	£ 3,867	$2.80 \cdot 10^{4}$ L	£ 0.023 L $^{-1}$	£ 644
Utility	Labour	$7.20 \cdot 10^{2}$ person·hr	£ 16.00 person^{-1} hr^{-1}	£ 11,520	$7.20 \cdot 10^{2}$ person·hr	£ 16.00 person^{-1} hr^{-1}	£ 11,520
Waste	Waste treatment	$1.20 \cdot 10^{4}$ L	£ 0.40·L $^{-1}$	£ 4,800	$1.70 \cdot 10^{4}$ L	£ 0.40·L $^{-1}$	£ 6,800
Capital Expenditure							
Equipment Purchase Cost (EPC)							
Cost component	Description	Quantity	Price	Cost	Quantity	Price	Cost
Equipment	Vessel material	12,000 L	£ 6598 $(L^{-1})^{0.6}$	£ 1,848,800	2,000 L	£ 6598 $(L^{-1})^{0.6}$	£630,960
Equipment	ATF filter	0 m^2	£ 68763 $(m^{-2})^{0.6}$	£ 0	2 m^2	£ 68763 $(m^{-2})^{0.6}$	£104,230
Direct / Indirect Cost (TDC / TIC)							
Cost component	Description	EPC value	Price	Cost	EPC value	Price	Cost
Direct	Installation	£ 1,848,803	£ 0.5·EPC	£ 924,401	£ 735,183	£ 0.5·EPC	£ 367,592
Direct	Process Piping	£ 1,848,803	£ 0.4·EPC	£ 739,521	£ 735,183	£ 0.4·EPC	£ 294,074
Direct	Instrumentation	£ 1,848,803	£ 0.35·EPC	£ 647,081	£ 735,183	£ 0.35·EPC	£ 257,314
Direct	Insulation	£ 1,848,803	£ 0.03·EPC	£ 55,464	£ 735,183	£ 0.03·EPC	£ 22,056
Direct	Electrical	£ 1,848,803	£ 0.15·EPC	£ 277,320	£ 735,183	£ 0.15·EPC	£ 110,278
Direct	Buildings	£ 1,848,803	£ 0.45·EPC	£ 831,961	£ 735,183	£ 0.45·EPC	£ 330,833
Direct	Maintenance	£ 1,848,803	£ 0.01·EPC	£ 18,488	£ 735,183	£ 0.01·EPC	£ 7,352
Indirect	Construction	£ 1,848,803	£ 0.35·EPC	£ 647,081	£ 735,183	£ 0.35·EPC	£ 257,314
Indirect	Contingency	£ 1,848,803	£ 0.50·EPC	£ 924,401	£ 735,183	£ 0.50·EPC	£ 367,592
Indirect	Contractors Fee	£ 1,848,803	£ 0.05·EPC	£ 92,440	£ 735,183	£ 0.05·EPC	£ 36,759

Total OpEx (per reactor per batch)	£ 168,939	£ 146,641
Total CapEx (per reactor)	£ 7,006,965	£ 2,786,347
Batches per year	22	22
Number of reactors	1	2
Total OpEx (per reactor)	£ 3,716,651	£ 3,226,091
Total OpEx	£ 3,716,651	£ 6,452,182
Total CapEx	£ 7,006,965	£ 5,572,693
Total first year cost	£ 10,723,616	£ 12,024,876
Total mAb produced	184.16 kg	238.51 kg

4. Discussion

Model-based process optimisation is of exceptional importance in Biopharma Industry 4.0 as discussed in recent reviews (Badr and Sugiyama, 2020; Papathanasiou and Kontoravdi, 2020). The present study offer quantitative corroboration of cost advantage opportunities by detailed technoeconomic comparisons. The fed-batch and then the perfusion reactor simulations are first discussed here, followed by the dynamic optimisation of both reactors and finally the key points of the technoeconomic analysis.

For fed-batch simulation, state variable trajectories are entirely dependent on the feeding strategy used. The strategy used here replicates that by De Tremblay et al. (1992), but any arbitrary strategy consisting of a variety pulses and steps of feed could be applied to the simulation. The first point of interest in the perfusion reactor simulation is the state steady behaviour of the reactor being achieved after 4 days, meaning additional feed had no effect on the final mAb titer. Altering the feeding strategy via redefining the bleed and harvest flows must be considered in order to improve final mAb concentration. Secondly, the reader must consider that the flowrate into the reactor was set equal to the total outlet flowrate. This strict constraint means once steady state is achieved no further state variable change will occur.

Various performance indicators (PIs) of interest could be used to form a brief comparison between the optimised fed-batch and perfusion reactors. The PIs considered were productivity, yield, final titer and total product produced for three products of interest (mAb, lactate and ammonia). This PI analysis for the FB-40-15 and P-40-15 designs can be visualised below in Table 15.

Table 15: Performance indicators of a single campaign of the FB-40-15 and P-40-15.

Product	PI	FB-40-15	P-40-15
mAb	Productivity (g $L^{-1}day^{-1}$)	0.047	0.021
	Yield (g $(10^6\,cell)^{-1}$)	$2.18\cdot10^{-5}$	$6.58\cdot10^{-5}$
	Final titer (g L^{-1})	697.57	206.67
	Total Product (kg)	8.37	5.26
Lactate	Productivity (g $L^{-1}day^{-1}$)	0.25	0.20
	Yield (g $(10^6\,cell)^{-1}$)	$1.19\cdot10^{-4}$	$6.34\cdot10^{-4}$
	Final titer (mM)	42.72	31.25
	Total Product (kg)	45.66	50.75
Ammonia	Productivity (g $L^{-1}day^{-1}$)	0.0038	0.0038
	Yield (g $(10^6\,cell)^{-1}$)	$1.80\cdot10^{-6}$	$1.21\cdot10^{-5}$
	Final titer (mM)	3.40	3.33
	Total Product (kg)	0.69	0.97

Table 15 shows from a performance perspective, the fed-batch reactor outperforms the perfusion reactor in terms of mAb productivity, yield and total product, however perfusion does obtain a larger cellular yield compared to fed-batch. These yield values should be of cautious optimism for investors interested in integrated continuous bioprocessing technologies; if the unit sizes were designed with equal cellular loading capacities it would be reasonable to expect perfusion to produce greater mAb quantities. Despite this, in the instance of FB-40-15, the optimiser trajectory meant gradual feeding of medium during the early stages of operation allowed for enough cellular yield to outperform P-40-15. It is important to note here that productivity was taken as a function of medium volume fed throughout the entire time domain. Consequently, the significant difference in productivity can be attributed to the amount of medium being fed to the perfusion reactor during operation; 15,000 L across the 15 day time domain. This result emphasises the importance of variation of the manipulated variable (inlet, harvest and bleed flowrate) constraints on the resulting optimised bioreactor performance. Analysis into the effect of these manipulated variables on mAb production is necessary in future studies.

On the other hand, the final lactate and ammonia titers are both reduced in the perfusion design. Lower ammonia concentrations have been shown to be beneficial to the N-linked glycosylation property exhibited in mAbs, a critical quality factor for molecular bioactive performance (Karst et al., 2017).

Furthermore, excess lactate accumulation, coupled with limited glucose access has been shown to lead to immature glycan production from mammalian cell cultures (Zhang et al., 2019). Both of these points indicate the fed-batch reactor may be susceptible to producing mAbs of lower therapeutic value than the perfusion mode bioreactor. Ultimately, these points highlight the need to analyse the quality of mAb glycans produced within both these systems, to establish if they can produce high-quality therapeutics.

Finally, we discuss some observations from the economic analysis. The model applied to construct the simulation and optimisation has some limitations which should not be disregarded. Model assumptions include negligible lag phase for the growth of cells, homogeneous temperature and concentration, the clean in place strategy and negligible contamination between campaigns, constant pH maintained throughout runs and no oxygen mass-transfer limitations in the systems. All of these assumptions would need to be heavily scrutinised in future studies to confirm their validity to replicate experimental data.

A substantial economic study comparing industrial scale optimised fed-batch and perfusion reactors was detailed in Section 3.6. The analysis of the operating cost breakdown of the fed-batch designs (Fig. 11) shows significant opportunity for OpEx reduction via cost effective sourcing of the cleaning products and applying a different mixing strategy. Currently nitric acid and sodium chloride are supplemented to the reactor as necessary components to the cleaning duty. If nitric acid and sodium chloride were substituted with alternative cleaning solutions at a lower price, significant economic enhancement would be anticipated. Further to this, the electrical demand for mixing of the 12,000 L fed-batch vessels is currently a serious hindrance to its operation. Opportunity for cost reduction could be found by sourcing a different agitator or reducing the mixing frequency. As for the perfusion reactor, the current designs rely heavily on the input of fresh medium to allow the culture to proliferate. An example of this is P-40-15, for which expenditure on the culture and medium alone accounts for 81.2% of perfusion OpEx (Fig. 11). It is important to note that due to the significant sum of the medium being fed in these industrial scale designs, even a marginal decease in the unit price of the medium could lead to significant savings in both modes of operation, particularly the perfusion designs.

NPC and COGS metrics were implemented in order to evaluate the long term sustainability of the design proposals and their ability to handle market pressures. The interest rate was shown to be a key parameter in the trend of the NPC towards the end of the plant life, however its effect was fairly limited in the early stages of operation. This point is evident when analysing the numerical economic data, at the 2nd year of operation of the P-40-15 bioreactor, a fixed 10% interest rate would lead to a relative NPC increase of 4% compared to a fixed 2% interest rate. By the 5th year of operation however, the relative NPC increase reaches 19% and at the point of decommissioning (year 15), the relative NPC increase reaches 110%. The relative NPC increase after 15 years is marginally smaller when considering fed-batch, reaching 104%. Ultimately, this analysis uncovered the actuality that both designs are highly susceptible to long term economic uncertainty, especially the perfusion design.

The COGS analysis supported the findings observed within the NPC trajectories in that high cell density designs provided greater economic prospects. It also clearly demonstrated the strongest design option from a mAb production standpoint was FB-40-15, since it produced the lowest average final year COGS values and consistently exhibited lower COGS values than the corresponding perfusion design (P-40-15) throughout majority of the interest rates and time domain considered. As indicated in the NPC analysis, the higher interest rate values begin to cause significant trouble to the later stage economic viability of both designs. The problem is especially pronounced in the 8-10% interest rate trajectory for perfusion designs (Fig. 14), however it is still prevalent in the 5% case. The cheapest COGS value encountered for P-40-15 for the 5% interest rate occurred at year 5 of operation, whilst for FB-40-15 it occurred at year 8 of operation. This suggests careful consideration should be made regarding the lifetime of these designs along with the flexibility of profit margin needed to operate viably. Further economic analysis considering historical trends of inflation trajectories as well as implementing dynamic interest rate parameters should be tested to uncover further economic insights.

Readers should note that despite exclusion of downstream units in this study, literature references generally cite downstream continuous separations as more cost effective than downstream batch separations (Yang et al., 2019). Many other references cite upstream continuous units having greater

productivity than their batch or fed-batch counterparts (Shirahata et al., 2019; Yang et al., 2019), however, in this study the opposite outcome was encountered – the optimised fed-batch bioreactor of choice (FB-40-15) outputted greater quantity of product per unit volume per unit time than either high cell density perfusion designs (P-40-15 and P-40-30). This outcome is in agreement with the recent study by (Badr et al., 2021), who highlighted that current upstream fed-batch mAb technologies hold greater economic promise than current upstream perfusion mAb technologies. Productivity levels for both designs is fundamental to COGS analyses. If technology surpasses model assumptions, inducing a perfusion benefit overfed-batch productivity, e.g. due to advanced control (Papathanasiou et al., 2019) then it may become more economically favourable to use and operate industrial scale perfusion reactors.

A point to consider here is that the single-objective optimisation method only addresses mAb maximisation from the bioreactors at the final time (or over the time horizon). This approach is in agreement with recent studies conducted for mAb bioreactors (Kiparissides et al. 2015; Kappatou et al., 2018). Beyond the current formulation, other factors can also be considered as implicit constraints for reactor optimisation, including the need for high cell viability and low harmful/waste by-products (e.g. ammonia, lactate) whose detrimental presence causes cell growth inhibition (Kappatou et al., 2018).

A key factor in any process engineering operation is operational uncertainty. It is essential to consider the likelihood of process failure, supply chain disruptions, etc. in process systems studies. (Pollock et al., 2013) applied Monte Carlo simulations in order to understand the probability of uncertainty in fed-batch and perfusion culture processes. The current study does not implement this measure, however, readers should consider it an important factor in assessing the prospective large scale viability of these reactor designs.

5. Conclusions

To understand the metabolic network within a hybridoma cell line used to manufacture mAbs, two dynamic simulations were constructed, one for a fed-batch reactor and one for a perfusion reactor. A single-objective dynamic optimisation is proposed, and the maximisation of total mAb production within the fed-batch and perfusion reactors is acchieved by solving for the decision (manipulated) inlet and outlet flow variables. A simultaneous finite approximation method was used to formulate the dynamic optimisation problem in the form of a NLP problem. Following this, the software library APOPT was used to solve the NLP problem for the fed-batch bioreactor, whilst IPOPT was used to solve for the perfusion system, elucidating optimal control trajectories. Lastly, a considerable effort has been made to quantify the cost implications of constructing these proposed designs via an economic analysis. The analysis highlighted that current upstream perfusion technologies still require further development in order to compete with their fed-batch counterparts, in full agreement with other recent studies (Badr et al., 2021). Future studies can address how product quality and quantity can be simultaneously pursued via bi-objective dynamic optimisation (Kontoravdi et al., 2007), while possibly also considering multi-parametric cell line behaviour (Alhuthali et al., 2021). Furthermore, future work should consider the integration of upstream unit operations to downstream unit operations to visualise plant-wide optimisation solutions (Chon and Zarbis-Papastoitsis, 2011). Rigorous methodologies for improved economic and environmental plant performance can also be pursued (Amasawa et al., 2021).

Author Information

Corresponding Author
Email: D.Gerogiorgis@ed.ac.uk
Phone: + *44 131 6517072*
ORCID ID: Dimitrios I. Gerogiorgis: 0000-0002-2210-6784

Acknowledgements

The authors gratefully acknowledge the Engineering and Physical Sciences Research Council (EPSRC) Doctoral Training Partnership (DTP) PhD Scholarship awarded to W.J., as well as a Royal Society Short Industrial Fellowship (2020-21) awarded to D.I.G.

Nomenclature and acronyms

A_{vessel}	Surface area of the reactor vessel (m^2)
$[AMM]$	Ammonia concentration (mol L^{-1})
AMM_G	Ammonia generated (mol)
$[AMM]_0$	Initial ammonia concentration (mol L^{-1})
CapEx	Capital expenditure (£)
C_A	Cost of equipment A (£)
C_B	Cost of equipment B (£)
$C_{electricity}$	Total cost of the electricity (£)
COGS	Cost of goods sold per gram (£/g)
C_{media}	Total cost of the media (£)
C_{RM}	Total cost of raw materials (£)
C_U	Total cost of utilities (£)
C_{WT}	Total cost of waste treatment (£)
c_p	Heat capacity (kJ kg^{-1} $C^{\circ-1}$)
$CU_{electricity}$	Cost unit for electricity (£ kWh^{-1})
CU_{media}	Cost per unit of media (£ mL^{-1})
D	Diameter of impeller (m)
D_F	Diameter of the fermenter (m)
EPC	Equipment purchase cost (£)
F_{bleed}	Bleed flowrate (L day^{-1})
$F_{harvest}$	Harvest flowrate (L day^{-1})
F_{in}	Flowrate into the reactor (L day^{-1})
F_{out}	Flowrate out of the reactor (L day^{-1})
g	Inequality constrained variable (-)
g_f	Inequality constrained variable (-)
$[GLC]$	Glucose concentration (mol L^{-1})
GLC_C	Glucose consumption (mol)
$[GLC]_{in}$	Glucose inlet concentration (mol L^{-1})
$[GLC]_0$	Initial glucose concentration (mol L^{-1})
$[GLN]$	Glutamine concentration (mol L^{-1})
GLN_C	Glutamine consumption (mol)
$[GLN]_{in}$	Glutamine inlet concentration (mol L^{-1})
$[GLN]_0$	Initial glutamine concentration (mol L^{-1})
h	Equality constrained variable (-)
h_f	Equality constrained variable at time = t_f (-)
H	Height of the fermenter (m)
k	Power constant (-)
k_d	Specific death rate (day^{-1})
$[LAC]$	Lactate concentration (mol L^{-1})
LAC_G	Lactate generated (mol)
$[LAC]_0$	Initial lactate concentration (mol L^{-1})
$[M](t)$	Material concentration in the reactor at time t (mol L^{-1})
M_f	Final material (mol)
$[M]_f$	Final material concentration (mol L^{-1})
M_F	Fed material (mol)
$\mathbf{M_i}$	Molar mass of material i (g/mol)
M_i	Initial material (mol)
$[M]_i$	Initial material concentration (mol L^{-1})
$M_{kg,i}$	Mass of material i in kilograms (kg)
$M_{mol,i}$	Mass of material i in moles (mol)
M_O	Outlet material (mol)
$[mAb]$	mAb concentration (mg L^{-1})

mAb_G	mAb generated (mol)
$[mAb]_0$	Initial monoclonal antibody concentration (mol L^{-1})
$\dot{m}_{solution}$	Mass flowrate of solution into the reactor (kg s^{-1})
N	Stirring speed (s^{-1})
N_p	Power number (-)
NPC	Net present cost (£)
OpEx	Operational expenditure (£)
$P_{heating}$	Total heating power (kWh)
P_{mixing}	Total mixing power (kWh)
P_{total}	Total electrical power (kWh)
q_{AMM}	Ammonia specific productivity (mol $cell^{-1}L^{-1}$)
q_{GLC}	Specific consumption rate of glucose (mol $cell^{-1}L^{-1}$)
q_{GLN}	Specific consumption rate of glutamine (mol $cell^{-1}L^{-1}$)
q_{LAC}	Lactate specific productivity (mol $cell^{-1}$ L^{-1})
q_{mAb}	Antibody specific productivity (mol $cell^{-1}L^{-1}$)
r	Annual interest rate(-)
Re	Reynolds number (-)
RVCC	Relative viable cell count (%)
S_A	Capacity of equipment A (m^2)
S_B	Capacity of equipment B (m^2)
t	Time (days)
TDC	Total direct cost (£)
t_f	Final time (-)
t_i	Initial time (-)
TIC	Total indirect cost (£)
ΔT	Difference between reactor and ambient temperature (˚C)
U	Overall heat transfer coefficient (W m^{-2} ˚C $^{-1}$)
$\boldsymbol{u}(t)$	Control vector at time *t* (-)
$\boldsymbol{u}(t)_L$	Control variable lower boundary vector (-)
$\boldsymbol{u}(t)_U$	Control variable upper boundary vector (-)
V	Working volume (L)
V_F	Volume of the fermenter tank (L)
V_f	Final culture medium volume (L)
V_i	Initial culture medium volume (L)
V_0	Initial volume (L)
$\boldsymbol{x}(t)$	State variable vector at time t (-)
$\boldsymbol{x}(t_f)$	State variable vector at the final time (-)
$\boldsymbol{x}(t_0)$	Initial state variable vector
$\boldsymbol{x_0}$	Initial state variable vector values
$\boldsymbol{x}(t)_L$	State variable lower boundary vector (-)
$\boldsymbol{x}(t)_U$	State variable upper boundary vector (-)
X_i	i^{th} state variable (-)
X_j	j^{th} state variable (-)
$[X_V]$	Viable cell density (cells L^{-1})
$X_{V,G}$	Viable cell generated (cells)
$X_{V,0}$	Initial viable cell concentration (cells L^{-1})
X_{V,t_f}	Final time viable cell concentration (cells L^{-1})
$\rho_{solution}$	Density of solution in the reactor (kg m^{-3})
τ	Process lifetime (years)
φ	Objective variable (-)
$\mu_{solution}$	Viscosity of solution in the reactor (Pa·s)
μ	Specific growth rate (day^{-1})

References

Ahangarzadeh, S., Z. Payandeh, R. Arezumand, K. Shahzamani, F. Yarian and A. Alibakhshi (2020). An update on antiviral antibody-based biopharmaceuticals. *International Immunopharmacology* **86**: 106760.

Alhuthali, S., P. Kotidis, C. Kontoravdi (2021). Osmolality effects on CHO cell growth, cell volume, antibody productivity and glycosylation, *International Journal of Molecular Sciences* **22**(7): 3290.

Amasawa, E., H. Kuroda, K. Okamura, S. Badr and H. Sugiyama (2021). Cost-benefit analysis of monoclonal antibody cultivation scenarios in terms of life cycle environmental impact and operating cost. *ACS Sustainable Chemistry & Engineering*. **9**: 14012-14021.

Badr, S., K. Okamura, N. Takahashi, V. Ubbenjans, H. Shirahata and H. Sugiyama (2021). Integrated design of biopharmaceutical manufacturing processes: Operation modes and process configurations for monoclonal antibody production. *Computers & Chemical Engineering* **153**: 107422.

Badr, S. and H. Sugiyama (2020). A PSE perspective for the efficient production of monoclonal antibodies: integration of process, cell, and product design aspects. *Current Opinion in Chemical Engineering* **27**: 121-128.

Balcarcel, R. R. and G. Stephanopoulos (2001). Rapamycin reduces hybridoma cell death and enhances monoclonal antibody production. *Biotechnology and Bioengineering* **76**(1): 1-10.

Banik, G. G. and C. A. Heath (1995). Partial and total cell retention in a filtration-based homogeneous perfusion reactor. *Biotechnology Progress* **11**(5): 584-588.

Bayer, V. (2019). An overview of monoclonal antibodies. *Seminars In Oncology Nursing*, Elsevier.

Bibila, T. A. and D. K. Robinson (1995). In pursuit of the optimal fed-batch process for monoclonal antibody production. *Biotechnology Progress* **11**(1): 1-13.

Biegler, L. T. (2007). An overview of simultaneous strategies for dynamic optimization. *Chemical Engineering and Processing: Process Intensification* **46**(11): 1043-1053.

Biegler, L. T. (2010). Nonlinear programming: concepts, algorithms, and applications to chemical processes, SIAM.

Bremer, P. J., S. Fillery and A. J. McQuillan (2006). Laboratory-scale Clean-In-Place (CIP) studies on the effectiveness of different caustic and acid wash steps on the removal of dairy biofilms. *International Journal of Food Microbiology* **106**(3): 254-262.

Buchi, J. R. and L. H. Landweber (1990). Solving sequential conditions by finite-state strategies. *The Collected Works of J. Richard Büchi*, Springer**:** 525-541.

Bunnak, P., R. Allmendinger, S. V. Ramasamy, P. Lettieri and N. J. Titchener-Hooker (2016). Life-cycle and cost of goods assessment of fed-batch and perfusion-based manufacturing processes for mAbs. *Biotechnology Progress* **32**(5): 1324-1335.

Chames, P., M. Van Regenmortel, E. Weiss and D. Baty (2009). Therapeutic antibodies: successes, limitations and hopes for the future. *British Journal of Pharmacology* **157**(2): 220-233.

Chemicals. (2021a). Nitric Acid. Retrieved from: Nitric Acid For Sale | Buy Nitric Acid Online | UK Suppliers (chemicals.co.uk)

Chemicals (2021b). Sodium Chloride. Retrieved from: Buy Sodium Chloride | Cheap UK Chemicals at ReAgent

Chen, J. and K.-P. Wang (2004). Sequential experimental design strategy for optimal batch profiles using hybrid function approximations. *Industrial & Engineering Chemistry Research* **43**(17): 5260-5274.

Chon, J. H. and G. Zarbis-Papastoitsis (2011). Advances in the production and downstream processing of antibodies. *New Biotechnology* **28**(5): 458-463.

Colombel, J. F., W. J. Sandborn, P. Rutgeerts, R. Enns, S. B. Hanauer, R. Panaccione, S. Schreiber, D. Byczkowski, J. Li and J. D. Kent (2007). Adalimumab for maintenance of clinical response and remission in patients with Crohn's disease: the CHARM trial. *Gastroenterology* **132**(1): 52-65.

De Tremblay, M., M. Perrier, C. Chavarie and J. Archambault (1992). Optimization of fed-batch culture of hybridoma cells using dynamic programming: single and multi feed cases. *Bioprocess Engineering* **7**(5): 229-234.

Del Moral, P., A. Doucet and A. Jasra (2012). On adaptive resampling strategies for sequential Monte Carlo methods. *Bernoulli* **18**(1): 252-278.

Diab, S., D.T. McQuade, F. Gupton and D. I. Gerogiorgis (2019). Process design and optimization for the continuous manufacturing of nevirapine, an active pharmaceutical ingredient for HIV treatment. *Organic Process Research & Development* **23**(3): 320-333.

Diab, S., S. Badr, H. Sugiyama and D. I. Gerogiorgis (2020). Dynamic Simulation and Visualisation of pH-Modulated fed-batch fermentation for mAb production from CHO cell cultures. *Computer Aided Chemical Engineering*, Elsevier. **48:** 1657-1662.

Ecker, D. M., S. D. Jones and H. L. Levine (2015). The therapeutic monoclonal antibody market. *MAbs*, Taylor & Francis.

Farid, S. S. (2007). Process economics of industrial monoclonal antibody manufacture. *Journal of Chromatography B* **848**(1): 8-18.

Franco-Lara, E. and D. Weuster-Botz (2005). Estimation of optimal feeding strategies for fed-batch bioprocesses. *Bioprocess and Biosystems Engineering* **27**(4): 255-262.

Furman, R. R., J. P. Sharman, S. E. Coutre, B. D. Cheson, J. M. Pagel, P. Hillmen, J. C. Barrientos, A. D. Zelenetz, T. J. Kipps and I. Flinn (2014). Idelalisib and rituximab in relapsed chronic lymphocytic leukemia. *New England Journal of Medicine* **370**(11): 997-1007.

Gerogiorgis, D. I. and P. I. Barton (2009). Steady-state optimization of a continuous pharmaceutical process. *Computer-Aided Chemical Engineering* **27**: 927-932.

Gerogiorgis, D. I. and H. G. Jolliffe (2015). Continuous pharmaceutical process engineering and economics: Investigating technical efficiency, environmental impact and economic viability. *Chimica Oggi-Chemistry Today* **33**(6): 29-32.

Goding, J. W. (1996). Monoclonal antibodies: principles and practice, Elsevier.

Green, D. W. and M. Z. Southard (2019). *Perry's Chemical Engineers' Handbook*, McGraw-Hill Education.

Grilo, A. L. and A. Mantalaris (2019). The increasingly human and profitable monoclonal antibody market. *Trends in Biotechnology* **37**(1): 9-16.

Han, W., J. Fang, Z. Liu and J. Tang (2016). Techno-economic evaluation of a combined bioprocess for fermentative hydrogen production from food waste. *Bioresource Technology* **202**: 107-112.

Johnson, M., P. J. Heggs and T. Mahmud (2016). Assessment of overall heat transfer coefficient models to predict the performance of laboratory-scale jacketed batch reactors. *Organic Process Research & Development* **20**(2): 204-214.

K Sinnott, R. (2005). Coulson & Richardson's Chemical Engineering Volume 6, Copyright.

Kabo, G. J., O. V. Voitkevich, A. V. Blokhin, S. V. Kohut, E. N. Stepurko and Y. U. Paulechka (2013). Thermodynamic properties of starch and glucose. *The Journal of Chemical Thermodynamics* **59**: 87-93.

Kappatou, C. D., A. Mhamdi, A. Q. Campano, A. Mantalaris and A. Mitsos (2018). Model-based dynamic optimization of monoclonal antibodies production in semibatch operation—Use of reformulation techniques. *Industrial & Engineering Chemistry Research* **57**(30): 9915-9924.

Kameswaran, S. and L. T. Biegler (2006). Simultaneous dynamic optimization strategies: Recent advances and challenges. *Computers & Chemical Engineering* **30**(10-12): 1560-1575.

Kantardjieff, A. and W. Zhou (2013). Mammalian cell cultures for biologics manufacturing. *Mammalian Cell Cultures for Biologics Manufacturing*, Springer**:** 1-9.

Karagiannis, I. C. and P. G. Soldatos (2008). Water desalination cost literature: review and assessment. *Desalination* **223**(1-3): 448-456.

Karst, D. J., E. Scibona, E. Serra, J. M. Bielser, J. Souquet, M. Stettler, H. Broly, M. Soos, M. Morbidelli and T. K. Villiger (2017). Modulation and modeling of monoclonal antibody N-linked glycosylation in mammalian cell perfusion reactors. *Biotechnology and Bioengineering* **114**(9): 1978-1990.

Kesik-Brodacka, M. (2018). Progress in biopharmaceutical development. *Biotechnology and Applied Biochemistry* **65**(3): 306-322.

Kiparissides, A., E. Pistikopoulos and A. Mantalaris (2015). On the model-based optimization of secreting mammalian cell (GS-NS0) cultures. *Biotechnology and bioengineering* **112**(3): 536-548.

Klutz, S., L. Holtmann, M. Lobedann and G. Schembecker (2016). Cost evaluation of antibody production processes in different operation modes. *Chemical Engineering Science* **141**: 63-74.

Kontoravdi, C., S. P. Asprey, E. N. Pistikopoulos and A. Mantalaris (2007). Development of a dynamic model of monoclonal antibody production and glycosylation for product quality monitoring. *Computers & Chemical Engineering* **31**(5-6): 392-400.

Lindskog, E. K. (2018). The upstream process: principal modes of operation. *Biopharmaceutical Processing*, Elsevier**:** 625-635.

Lira-Parada, P. A., E. Pettersen, L. T. Biegler and N. Bar (2021). Implications of dimensional analysis in bioreactor models: Parameter estimation and identifiability. *Chemical Engineering Journal*: 129220.

Lu, R.-M., Y.-C. Hwang, I.-J. Liu, C.-C. Lee, H.-Z. Tsai, H.-J. Li and H.-C. Wu (2020). Development of therapeutic antibodies for the treatment of diseases. *Journal of Biomedical Science* **27**(1): 1-30.

Luedeking, R. and E. L. Piret (2000). A kinetic study of the lactic acid fermentation. Batch process at controlled pH. *Biotechnology and Bioengineering* **67**(6): 636-644.

Mahmuda, A., F. Bande, K. J. K. Al-Zihiry, N. Abdulhaleem, R. Abd Majid, R. A. Hamat, W. O. Abdullah and Z. Unyah (2017). Monoclonal antibodies: A review of therapeutic applications and future prospects. *Tropical Journal of Pharmaceutical Research* **16**(3): 713-722.

Mannina, G., M. Alliet, C. Brepols, J. Comas, J. Harmand, M. Heran, N. Kalboussi, J. Makinia, Á. Robles and T. F. Rebouças (2021). Integrated membrane bioreactors modelling: a review on new comprehensive modelling framework. *Bioresource Technology*: 124828.

Morchain, J. and C. Fonade (2009). A structured model for the simulation of bioreactors under transient conditions. *AIChE Journal* **55**(11): 2973-2984.

Musarat, M. A., W. S. Alaloul and M. Liew (2021). Impact of inflation rate on construction projects budget: A review. *Ain Shams Engineering Journal* **12**(1): 407-414.

Mutturi, S. (2018). Dynamic optimization of fed-batch bioprocesses using flower pollination algorithm. *Bioprocess and Biosystems Engineering* **41**(11): 1679-1696.

National Center for Biotechnology Information (2021a). PubChem Compound Summary for CID 5961, Glutamine. Retrieved November 15, 2021 from https://pubchem.ncbi.nlm.nih.gov/compound/Glutamine.

National Center for Biotechnology Information (2021b). PubChem Compound Summary for CID 91435, Lactate. Retrieved November 15, 2021 from https://pubchem.ncbi.nlm.nih.gov/compound/Lactate.

Nelson, A. L., E. Dhimolea and J. M. Reichert (2010). Development trends for human monoclonal antibody therapeutics. *Nature Reviews Drug Discovery* **9**(10): 767-774.

Newell, B., J. Bailey, A. Islam, L. Hopkins and P. Lant (1998). Characterising bioreactor mixing with residence time distribution (RTD) tests. *Water Science and Technology* **37**(12): 43-47.

Nguang, S. K., L. Chen and X. D. Chen (2001). Optimisation of fed-batch culture of hybridoma cells using genetic algorithms. *ISA Transactions* **40**(4): 381-389.

Niamsuwan, S., P. Kittisupakorn and I. M. Mujtaba (2011). Minimization of water and chemical usage in the cleaning in place process of a milk pasteurization plant. *Songklanakarin Journal of Science & Technology* **33**(4).

Okkels, F., M. Dufva and H. Bruus (2011). Optimal homogenization of perfusion flows in microfluidic bio-reactors: A numerical study. *PLoS One* **6**(1): e14574.

Assisting continuous biomanufacturing through advanced control in downstream purification

Papathanasiou, M.M., B. Burnak, J. Katz, N. Shah and E.N. Pistikopoulos (2019). Assisting continuous biomanufacturing through advanced control in downstream purification. *Computers & Chemical Engineering* **125**: 232-248.

Papathanasiou, M.M. and C. Kontoravdi (2020). Engineering challenges in therapeutic protein product and process design. *Current Opinion in Chemical Engineering* **27**: 81-88.

Pearson, A. (2008). Refrigeration with ammonia. *International Journal of Refrigeration* **31**(4): 545-551.

Petrides, D. (2000). Bioprocess design and economics. *Bioseparations Science and Engineering*: 1-83.

Pinelli, D., Z. Liu and F. Magelli (2010). Analysis of KLa measurement methods in stirred vessels: the role of experimental techniques and fluid dynamic models. *International Journal of Chemical Reactor Engineering* **8**(1).

Pollock, J., S. V. Ho and S. S. Farid (2013). Fed-batch and perfusion culture processes: economic, environmental, and operational feasibility under uncertainty. *Biotechnology and Bioengineering* **110**(1): 206-219.

Saeed, A. and S. Awan (2016). Advances in monoclonal antibodies production and cancer therapy. *MOJ Immunol* **3**(4): 00099.

Saraiva, I., A. V. Wouwer and A.-L. Hantson (2015). Parameter identification of a dynamic model of CHO cell cultures: an experimental case study. *Bioprocess and Biosystems Engineering* **38**(11): 2231-2248.

Sbarciog, M., D. Coutinho and A. V. Wouwer (2014). A simple output-feedback strategy for the control of perfused mammalian cell cultures. *Control Engineering Practice* **32**: 123-135.

Schaber, S. D., D. I. Gerogiorgis, R. Ramachandran, J. M. Evans, P. I. Barton and B. L. Trout (2011). Economic analysis of integrated continuous and batch pharmaceutical manufacturing: a case study. *Industrial & Engineering Chemistry Research* **50**(17): 10083-10092.

Scott, A. M., J. P. Allison and J. D. Wolchok (2012). Monoclonal antibodies in cancer therapy. *Cancer Immunity Archive* **12**(1).

Shirahata, H., S. Diab, H. Sugiyama and D. I. Gerogiorgis (2019). Dynamic modelling, simulation and economic evaluation of two CHO cell-based production modes towards developing biopharmaceutical manufacturing processes. *Chemical Engineering Research and Design* **150**: 218-233.

Smith, D. R. (1998). Variational methods in optimization, Courier Corporation

Spearman, M., B. Dionne and M. Butler (2011). The role of glycosylation in therapeutic antibodies. *Antibody Expression and Production*, Springer**:** 251-292.

Vermasvuori, R. and M. Hurme (2011). Economic comparison of diagnostic antibody production in perfusion stirred tank and in hollow fiber bioreactor processes. *Biotechnology Progress* **27**(6): 1588-1598.

Walsh, G. (2018). Biopharmaceutical benchmarks 2018. *Nature Biotechnology* **36**(12): 1136-1145.

Wells, J. A., A. R. Glassman, A. R. Ayala, L. M. Jampol, L. P. Aiello, A. N. Antoszyk, B. Arnold-Bush, C. W. Baker, N. M. Bressler and D. J. Browning (2015). Aflibercept, bevacizumab, or ranibizumab for diabetic macular edema. *The New England Journal of Medicine* **372**(13): 1193-1203.

Welty, J., G. L. Rorrer and D. G. Foster (2020). Fundamentals of momentum, heat, and mass transfer, John Wiley & Sons.

Woods, D. R. (2007). *Rules of Thumb in Engineering Practice*, John Wiley & Sons.

Woodside, S. M., B. D. Bowen and J. M. Piret (1998). Mammalian cell retention devices for stirred perfusion bioreactors. *Cytotechnology* **28**(1): 163-175.

Yang, O., S. Prabhu and M. Ierapetritou (2019). Comparison between batch and continuous monoclonal antibody production and economic analysis. *Industrial & Engineering Chemistry Research* **58**(15): 5851-5863.

Zeberli, A., G. Casola, S. Badr, C. Siegmund, M. Mattern and H. Sugiyama (2020). Approach for Multicriteria Equipment Redesign in Sterile Manufacturing of Biopharmaceuticals. *Journal of Pharmaceutical Innovation* **15**(1): 15-25.

Zhang, L., A. Castan, J. Stevenson, N. Chatzissavidou, F. Vilaplana and V. Chotteau (2019). Combined effects of glycosylation precfWursors and lactate on the glycoprofile of IgG produced by CHO cells. *Journal of Biotechnology* **289**: 71-79.

Zienkiewicz, O. C., K. Morgan and K. Morgan (2006). Finite elements and approximation, Courier Corporation.

Zürcher, P., H. Shirahata, S. Badr and H. Sugiyama (2020). Multi-stage and multi-objective decision-support tool for biopharmaceutical drug product manufacturing: Equipment technology evaluation. *Chemical Engineering Research and Design* **161**: 240-252.